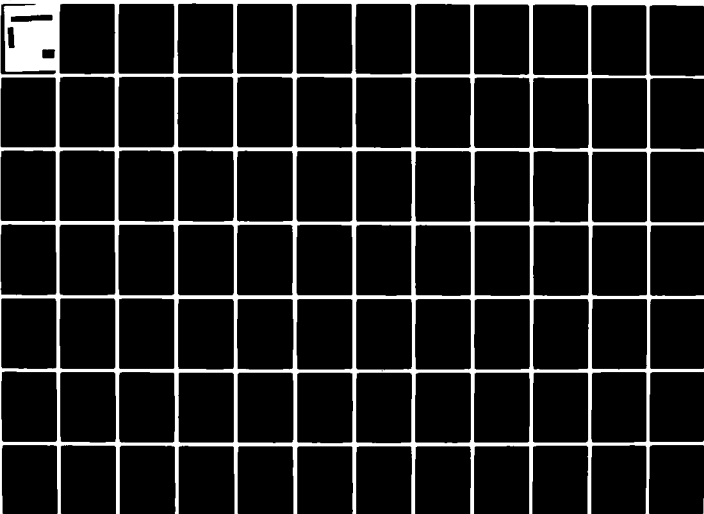


AD-A079 594

WASHINGTON UNIV ST LOUIS MO SEMICONDUCTOR RESEARCH LAB F/6 20/12
IMPURITY AND DEFECT BEHAVIOR IN HIGH-PURITY EPITAXIAL GaAs.(U)
SEP 79 C M WOLFE, K H NICHOLS AFOSR-76-2950
59356-6 AFOSR-TR-79-1326 NL

UNCLASSIFIED

1 - 2
AD
59356-6



DISTRIBUTION STATEMENT A

Approved for public release
Distribution Unlimited

WVLL # ACCE 116

ADA 079594

DDIC
RECEIVED
JAN 18 1980
A

Unclassified

SECURITY CLASSIFICATION OF THIS PAGE (When Data Entered)

REPORT DOCUMENTATION PAGE		READ INSTRUCTIONS BEFORE COMPLETING FORM
1. REPORT NUMBER 18 AFOSR-TR-79-1326	2. GOVT ACCESSION NO.	3. RECIPIENT'S CATALOG NUMBER
4. TITLE (and Subtitle) Impurity and Defect Behavior in High-Purity Epitaxial GaAs	5. TYPE OF REPORT & PERIOD COVERED Final Rept. 1 Jan 76-31 May 79	6. PERFORMING ORG. REPORT NUMBER 59356-6
7. AUTHOR(s) C. M. Wolfe & K. H. Nichols	8. CONTRACT OR GRANT NUMBER(s) AFOSR-76-2950	
9. PERFORMING ORGANIZATION NAME AND ADDRESS Washington University Box 1127 St. Louis, Mo. 63130	10. PROGRAM ELEMENT, PROJECT, TASK AREA & WORK UNIT NUMBERS 61102F 2306/B1	
11. CONTROLLING OFFICE NAME AND ADDRESS Air Force Office of Scientific Research/ Building 410 Bolling Air Force Base, DC 20332	12. REPORT DATE 26 Sep 79	13. NUMBER OF PAGES 127
14. MONITORING AGENCY NAME & ADDRESS (if different from Controlling Office) 12) 432	15. SECURITY CLASS. (of this report) Unclassified	15a. DECLASSIFICATION/DOWNGRADING SCHEDULE
16. DISTRIBUTION STATEMENT (of this Report) Approved for public release; distribution unlimited.		
17. DISTRIBUTION STATEMENT (of the abstract entered in Block 20, if different from Report)		
18. SUPPLEMENTARY NOTES		
19. KEY WORDS (Continue on reverse side if necessary and identify by block number) Epitaxial GaAs, impurity gradients, interfacial regions, self-compensation, impurity incorporation.		
20. ABSTRACT (Continue on reverse side if necessary and identify by block number) Although a number of mechanisms have been proposed to explain the existence of impurity gradients in epitaxial GaAs, the impurity gradient model presented in this report shows that such effects are inherent to the growth process. That is, when the carrier concentrations in the substrate, growing layer, and at the growth surface are different at the growth temperature, non-uniform time-dependent electric fields are obtained in the layer. These		

411 361

Unclassified

Unclassified

SECURITY CLASSIFICATION OF THIS PAGE(When Data Entered)

fields can enhance or retard the motion of ionized impurities and defects during growth, producing impurity gradients at the outer surface and different conductivity regions at the epitaxy-substrate interface.

High temperature resistivity and Hall coefficient measurements were made on epitaxial layers and substrates and analyzed using a self-consistent four-band model to obtain quantitative results for the impurity gradient model for growth on heavily-doped n-type substrates predicts that thin (0.05 μm or larger) p-type regions at the epitaxy-substrate interface will be produced under conditions commonly encountered in the epitaxial growth of GaAs.

Zero-bias capacitance measurements on Schottky barrier diodes reveal the presence of heavily-doped n-type regions near the outer surface. These surface gradients caused by surface states are predicted by the model. The effects of surface states can also explain the observed self-compensation in GaAs.

Unclassified

TABLE OF CONTENTS

No.	Page
1. Introduction	1
2. High-Temperature Carrier Transport.....	11
2.1 Epitaxial Layers.....	11
2.1.1 Experiment.....	13
2.1.1.1 Sample Preparation.....	13
2.1.1.2 Measurement Apparatus.....	14
2.1.1.3 Experimental Results.....	17
2.1.2 Analysis.....	24
2.1.2.1 Energy Separations.....	24
2.1.2.2 Four-Band Model.....	27
2.1.2.3 Effective Masses.....	28
2.1.2.4 Hall Coefficient.....	30
2.1.2.4.1 Extrinsic Conductivity	30
2.1.2.4.2 Intrinsic Conductivity	34
2.1.2.5 Resistivity.....	35
2.1.3 Conclusions.....	38
2.2 Substrates.....	40
3. Impurity Gradient Model.....	47
3.1 Time-Dependent Analysis.....	47
3.1.1 Electric Field.....	47
3.1.2 Impurity Concentrations.....	50
3.2 Time-Independent Solutions.....	52
3.2.1 Heavily-Doped Substrate.....	52
3.2.1.1 Assumptions.....	52
3.2.1.2 Electron Concentration.....	53
3.2.1.2.1 Solution.....	53
3.2.1.2.2 Boundary Conditions...	56
3.2.1.3 Electric Field.....	58
3.2.1.3.1 Interface.....	58
3.2.1.3.2 Surface.....	61
3.2.1.4 Impurity Concentrations.....	64
3.2.2 High Resistance Substrate.....	71
3.2.2.1 Intrinsic Layer.....	71
3.2.2.2 Extrinsic Layer.....	72
3.2.2.3 Chromium Impurity Gradient.....	74

AIR FORCE RESEARCH AND DEVELOPMENT COMMAND (AFRDC)
 NOTED
 TIME
 and
 DISTRICT
 A. D. [unclear]
 Technical [unclear]

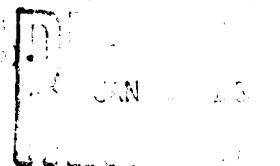


TABLE OF CONTENTS
(continued)

No.	Page
4. Surface State Effects.....	83
4.1 Surface Impurity Gradients.....	83
4.1.1 Analysis.....	83
4.1.2 Experiment.....	89
4.1.2.1 Heavily-Doped Substrate.....	89
4.1.2.2 Chromium-Doped Substrate.....	91
4.2 Self-Compensation Effect.....	94
4.2.1 Experiment.....	94
4.2.2 Analysis.....	97
4.2.2.1 Mass Action Laws.....	97
4.2.2.2 Charge Neutrality.....	
4.2.2.3 Surface States.....	
4.3 Conclusions.....	
5. Summary and Conclusions.....	
6. Acknowledgements.....	
7. Bibliography.....	
8. Vita.....	

Account Number	
NBS 2011	
INDEX	
UNIVERSITY	
RESEARCH	
A	

LIST OF TABLES

No.	Page
2.1	Sample Properties..... 18
2.2	Energies and temperature dependence of the Γ_6^C , L_6^C and X_6^C conduction-band minima of GaAs relative to the top of the valence band, Γ_8^V 26
4.1	Zero-bias capacitance for etched and as-grown epitaxial layers grown on n^+ substrates and the surface state densities at 1000 K needed to produce these data..... 90
4.2	Zero-bias capacitance for etched and as-grown epitaxial layers grown on Cr-doped substrates..... 92

LIST OF FIGURES

No.	Page
1.1 Carrier concentration versus distance from the surface for an n-type epitaxial layer grown on an n^+ substrate with a p-type interfacial region....	3
1.2 Carrier concentration versus epitaxial layer thickness for an n-type epitaxial layer grown on a Cr-doped substrate with an n^+ interfacial region.....	4
1.3 Net donor concentration ($N_d - N_a$) versus total impurity concentration ($N_d + N_a$).....	6
1.4 Energy band diagrams for (a) a heavily-doped substrate and (b) a Cr-doped substrate at the growth temperature (1000 K) and 300 K.....	8
2.1 Schematic of apparatus used for high-temperature resistivity and Hall measurements.....	15
2.2 Reciprocal of Hall coefficient times the elementary charge as a function of temperature for three GaAs epitaxial samples.....	21
2.3 Measured mobility, R_H/ρ , versus temperature for three GaAs epitaxial samples.....	22
2.4 Ratio of the mobility in the L_6^C minima to the mobility in the Γ_6^C minimum as a function of temperature for Samples No. 1 (O) and No. 2 (□).....	33

LIST OF FIGURES
(continued)

No.		Page
2.5	Mobilities in the Γ_6^C minimum, L_6^C minima and Γ_8^V maxima as a function of temperature for Samples No. 1 (O) and No. 2 (□).....	37
2.6	Four-band carrier concentration as a function of temperature for GaAs epitaxial Samples No. 1 (O), No. 2 (□) and No. 3 (Δ).....	39
2.7	Reciprocal of Hall coefficient times the elementary charge as a function of temperature for three Cr-doped GaAs substrates.....	43
2.8	Measured mobility, R_H/ρ , versus temperature for three Cr-doped GaAs substrates.....	44
2.9	Four-band electron concentration as a function of temperature for three Cr-doped GaAs substrates.....	45
3.1	Electron concentration versus distance for various substrate-intrinsic concentration ratios, N_s/n_i	59
3.2	Normalized electric field versus distance for various substrate-intrinsic concentration ratios, N_s/n_i	62
3.3	Variation of donor N_d and acceptor N_a concentrations with distance in the epitaxial layer at the growth temperature.....	66

LIST OF FIGURES
(continued)

No.	Page
3.4 Variation of the net donor concentration ($N_d - N_a$) with distance in the epitaxial layer at room temperature for several compensation ratios.....	68
3.5 Variation of donor N_d , acceptor N_a , and chromium N_{Cr} concentrations with distance in the epitaxial layer at the growth temperature.....	79
3.6 Variation of the net donor concentration ($N_d - N_a - N_{Cr}$) with distance in the epitaxial layer at room temperature for several chromium concentrations.....	80
4.1 Net donor concentration ($N_d - N_a$) for as-grown and etched epitaxial layers.....	84
4.2 Variation of the donor concentration (N_d) and the acceptor concentration (N_a) with the total ionized impurity concentration ($N_d + N_a$) for the column-IV impurities: Si, Ge, and Sn.....	95
4.3 Net donor concentration ($N_d - N_a$) versus total ionized impurity concentration ($N_d + N_a$).....	

1. INTRODUCTION

Since epitaxial layers of GaAs were first used [1] for the fabrication of Gunn oscillators, the occurrence of different conductivity regions at the layer-substrate interface [2,3] has been a recurring problem in the fabrication of GaAs microwave devices. To explain these interfacial regions a number of mechanisms have been proposed including outdiffusion or autodoping of amphoteric impurities from the substrate [2], defects formed by transient effects during the initial stages of growth [4], copper contamination of the substrate [5], substrate decomposition prior to growth [6,7], and a large concentration of silicon at the interface from the quartz reactor [8]. The impurity gradient model presented in this report shows that such interfacial regions are inherent to the growth process. That is, if all other possible mechanisms for the formation of interfacial regions were eliminated, in most epitaxial growth situations of practical interest these regions would still be observed.

The types of interfacial regions observed for growth on heavily-doped substrates are either high-resistivity n-type or p-type regions with thicknesses anywhere from about 5 μm to less than 0.1 μm [2,4-13]. It has been

* The numbers in parentheses in the text indicate references in the Bibliography.

shown, however, that the thicker high-resistance n-type regions are more properly interpreted as thin p-type regions [12,13]. The impurity gradient model presented in this report predicts a thin ($0.05 \mu\text{m}$ or larger) p-region at the layer-substrate interface under conditions commonly encountered in epitaxial growth. Figure 1.1, from the data of Sato and Iido [10], shows the type of interfacial region predicted by the model. At the interface between the n-type epitaxial layer and the n^+ substrate, there is a p-region approximately $0.05 \mu\text{m}$ thick. The observed profile is due to the outdiffusion of electrons and the fact that differential capacitance measurements measure the carrier concentration, not the net impurity concentration [14].

The types of interfacial regions commonly observed for growth on chromium-doped substrates are both p-type [15] and n-type [3]. Figure 1.2, from the data of Yamasaki [16], shows the type of heavier doped n-region predicted by the impurity gradient model. The profile in Figure 1.2 is due to the outdiffusion of electrons from a $0.05 \mu\text{m}$ heavier-doped region. The thickness of this interfacial region is very close to that predicted by the impurity gradient model.

This model can also explain the screening, above the intrinsic carrier concentration, of the donor-acceptor impurity interaction during incorporation into the epitaxial layer. That is, when the impurity concentrations are sufficiently below the intrinsic concentration, the

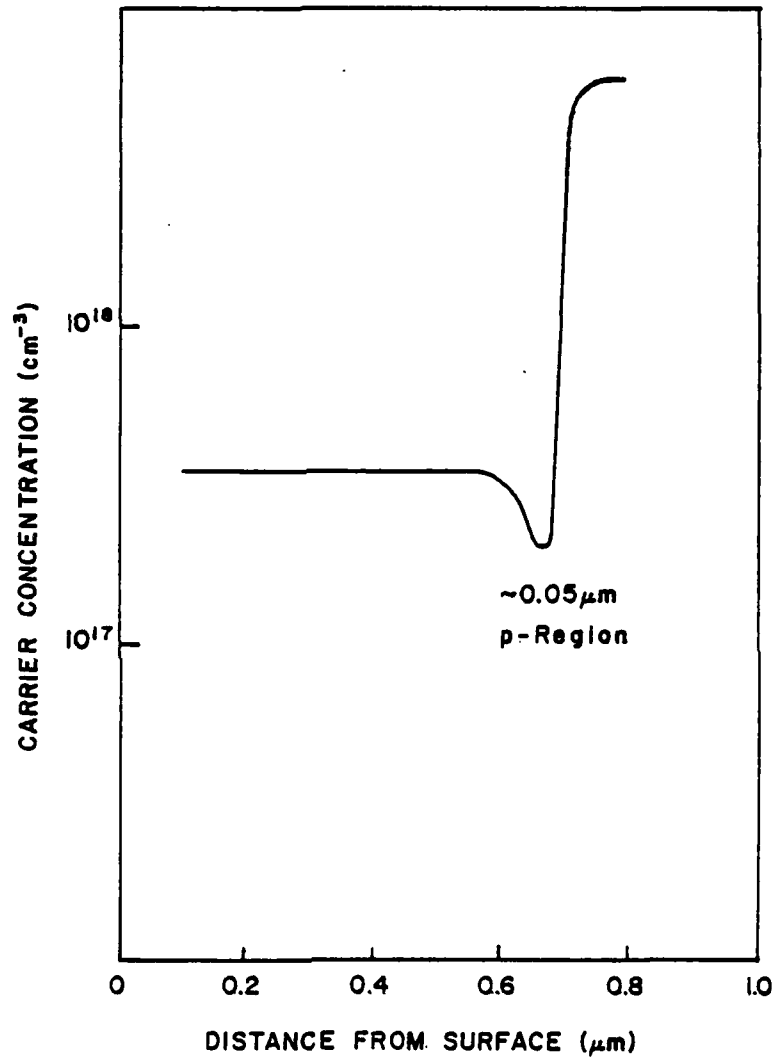


Figure 1.1 Carrier concentration versus distance from the surface for an n-type epitaxial layer grown on an n⁺ substrate with a p-type interfacial region.

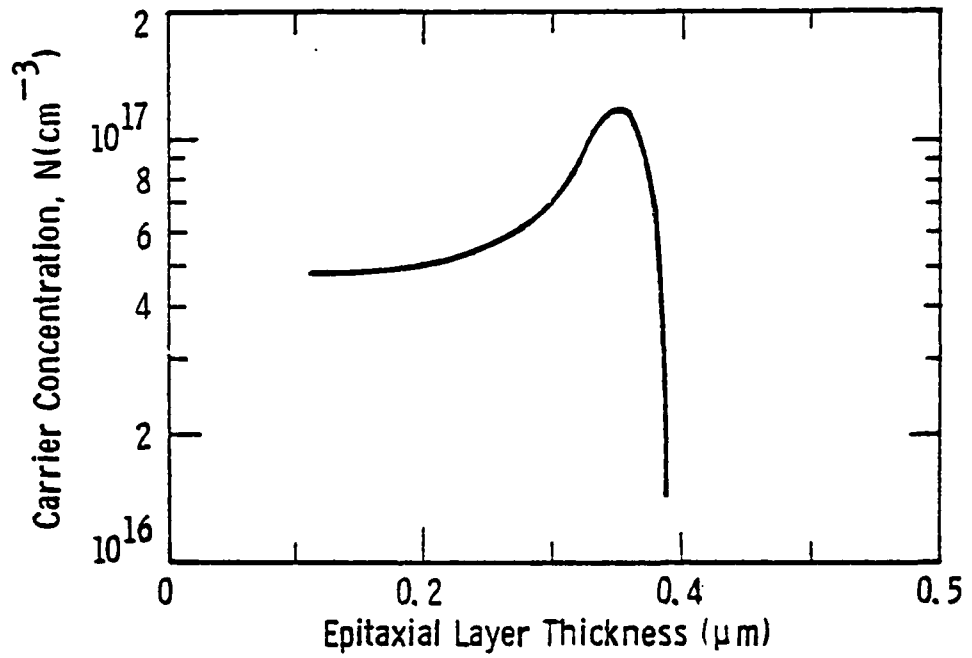


Figure 1.2 Carrier concentration versus epitaxial layer thickness for an n-type epitaxial layer grown on a Cr-doped substrate with an n^+ interfacial region.

impurities are screened by the intrinsic concentration. This produces a constant compensation ratio, N_a/N_d . However, when the impurity concentrations are above the intrinsic concentration, the donors and acceptors are expected to interact causing the compensation to increase. The dashed curve in Figure 1.3 is for the equilibrium condition where there is no variation between the electron concentration at the surface and inside the epitaxial layer. As can be seen, this dashed curve (no surface states) does not agree with the experimental data. On the other hand, band bending [17,18] at the surface, due to a lower electron concentration at the surface caused by surface states, can screen the donor-acceptor impurity interaction at higher concentrations. The solid curve in Figure 1.3 was fit to the experimental data by assuming the presence of $6.3 \times 10^{11} \text{ cm}^{-2}$ surface states.

The impurity gradient model can also explain the chromium pile-up observed at the surface of annealed, chromium-doped substrates [19,20,21] and epitaxial layers grown on chromium-doped substrates [22,23]. Since chromium has a charge of +2 in its compensating state and +3 in its neutral state [24], the electric field in the surface region will cause the chromium atoms to drift towards the surface. This drift will produce a chromium gradient at the surface with a thickness on the order of 0.10 μm .

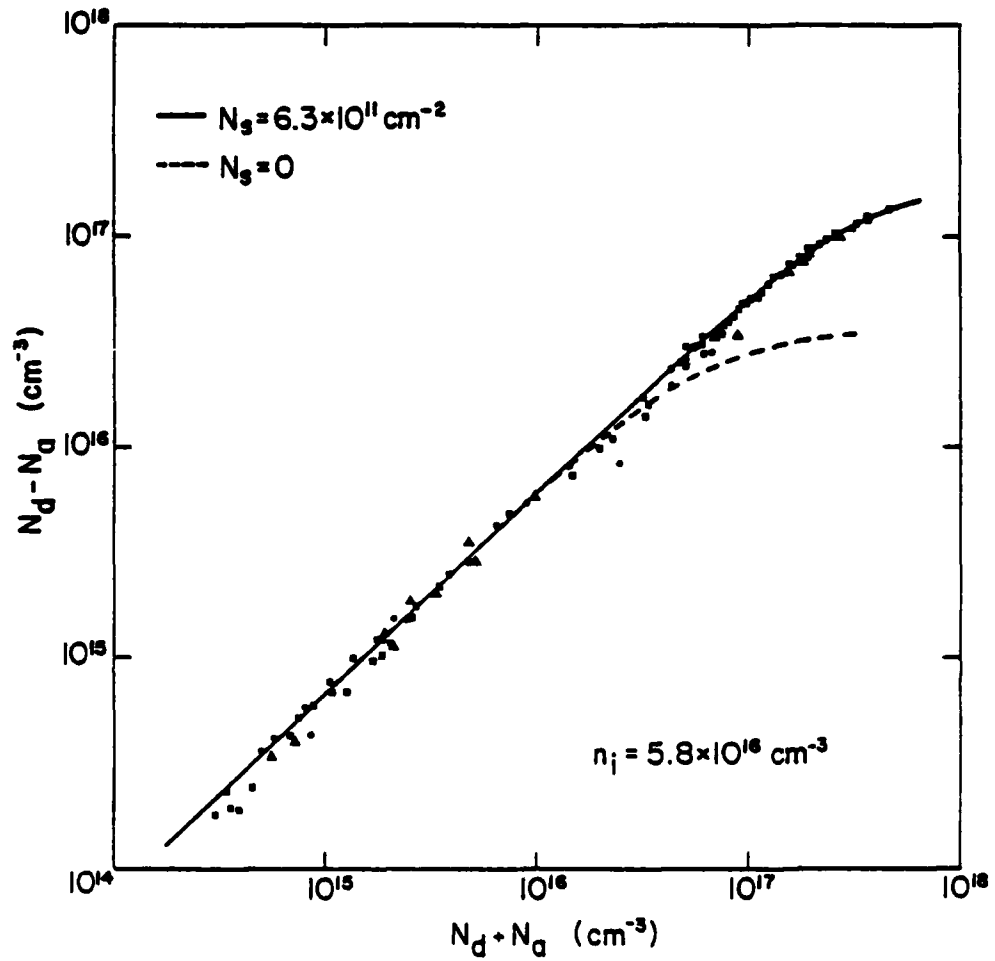


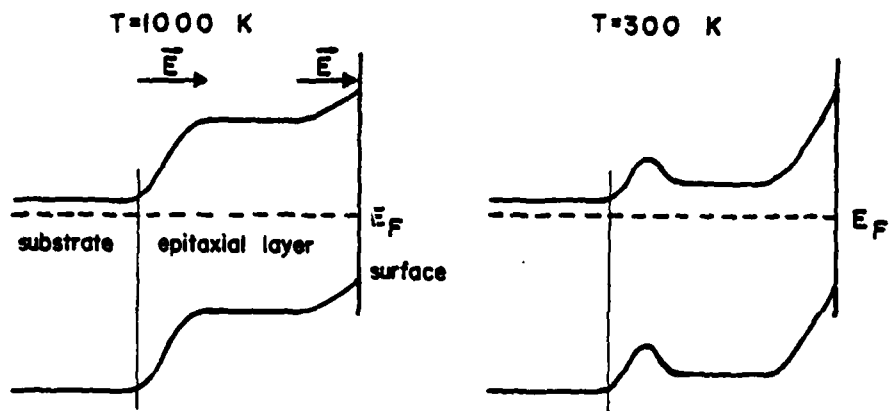
Figure 1.3 Net donor concentration ($N_d - N_a$) versus total ionized impurity concentration ($N_d + N_a$). The dashed line is calculated for zero surface states. The solid line is calculated for $6.3 \times 10^{11} \text{ cm}^{-2}$ surface states. The layers are doped with the column-IV impurities: Si (\bullet), Ge (\blacktriangle), and Sn (\blacksquare).

The salient features of the impurity gradient model for two sets of growth conditions are shown in Figure 1.4.

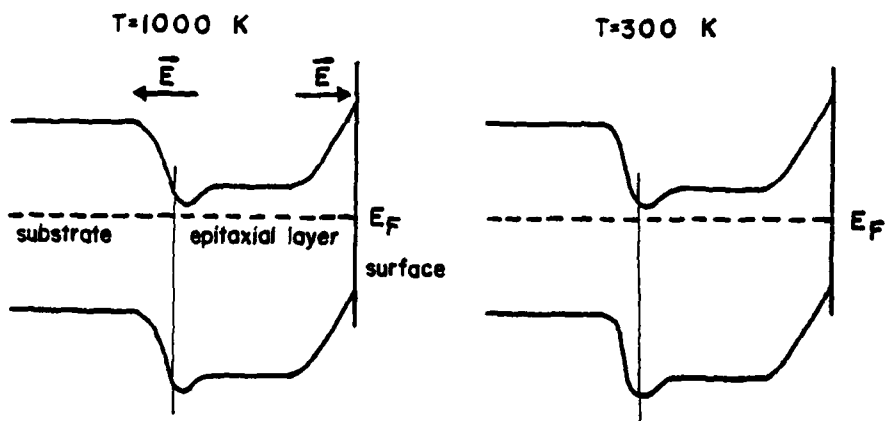
Figure 1.4 (a) is for the growth of a lightly doped epitaxial layer, which is intrinsic at 1000 K, on a heavily-doped substrate. At 1000 K the substrate is still extrinsic and the resulting difference in electron concentration produces an electric field between the substrate and the epitaxial layer. There is a similar electric field between the epitaxial layer and the surface caused by the lower electron concentration at the surface due to surface states. These electric fields will cause the positively-charged donors to drift away from the substrate-epitaxial layer interface and towards the surface. Similarly, the negatively-charged acceptors will drift away from the surface and towards the substrate-layer interface. This will produce a donor pile-up at the surface and an acceptor pile-up at the interface.

If this profile is frozen-in when the growth process is terminated, at 300 K a p-region will be formed at the substrate-layer interface. At the surface there will still be band bending due to surface states but the band bending will be reduced due to the heavier-doped region produced by the donor impurity gradient.

Figure 1.4 (b) indicates an epitaxial layer, which is extrinsic at 1000 K, being grown on a chromium-doped



(a)



(b)

Figure 1.4 Energy band diagrams for (a) a heavily-doped substrate and (b) a Cr-doped substrate at the growth temperature (1000 K) and 300K. The impurity gradients formed at 1000 K are assumed to be frozen in when the layer is cooled.

substrate, which is either slightly p-type or intrinsic at the growth temperature. The difference in electron concentration will produce a net electric field between the epitaxial layer and the substrate. There will also be band bending at the surface due to surface states similar to that previously discussed. This band bending will result in an electric field which will cause positively-charged donors to drift towards the surface and negatively-charged acceptors to drift away. In a similar manner, the electric field at the interface will cause the donors to drift towards the interface and the acceptors away.

If this profile is frozen in when the growth process is terminated, at 300 K heavier-doped regions will result at both the surface and substrate-epitaxial layer interface. Thus, the band bending at the surface will be reduced due to these impurity gradients.

This impurity gradient model predicts a surface impurity gradient which has not previously been reported in the literature. This surface gradient should occur in all n-type epitaxial layers which are doped below approximately 10^{18} cm^{-3} .

In this report, high temperature Hall and resistivity measurements on epitaxial layers and substrates will be discussed in Section 2. From these data the carrier concentrations of the epitaxial layers and substrates

can be calculated. Using these results a quantitative impurity gradient model will be discussed in Section 3. From the model a surface impurity gradient is predicted. In Section 4.1 the surface state density needed to form the experimentally observed surface impurity gradients will be calculated. This value will then be compared to the surface state density necessary to produce the experimentally measured compensation seen in GaAs. As will be seen, the good agreement between these two independently-obtained values tends to confirm the impurity gradient model.

2. HIGH-TEMPERATURE CARRIER TRANSPORT

2.1 EPITAXIAL LAYERS

High temperature Hall measurements are important, not only for the insights they give into band structure parameters, but also because of the data they provide for modeling epitaxial growth phenomena [25] and other high temperature processing. Earlier high temperature Hall measurements were made on polycrystalline [26] or bulk grown GaAs [27-30]. To improve the quality of these data, more recent measurements have been made on higher-purity epitaxial GaAs layers [31-35]. For room-temperature electrical measurements, epitaxial layers are grown on Cr-doped substrates with a room temperature resistivity of approximately $10^8 \Omega\text{-cm}$. Since the purest n-type layers have a resistivity of only about $50 \Omega\text{-cm}$, the conduction through the substrate is negligible. This substrate, however, provides severe restrictions to high-temperature electrical measurements on epitaxial material due to a rapid increase in the conductivity of the substrate. Zucca [36] has measured a decrease in resistivity of $10^4 \Omega\text{-cm}$ when Cr-doped substrates were heated from 300 to 500 K. Allen [37] has observed an increase of 10^6 in the carrier concentration of Cr-doped GaAs when heated from 300 to 600 K, thereby reducing the resistivity to only

$10^2 \Omega\text{-cm}$. This substrate conduction can make the parallel current paths of the epitaxial layer and substrate of comparable resistance, thus strongly affecting the measured electrical properties of epitaxial layers above 500 K. Much of the recent data on epitaxial layers have been obtained with the substrates still attached [31 33]. Although anomalous features observed have been attributed to deep donors, some of these results are probably due to conduction in the substrate.

Akita *et al.* [34] have briefly reported measurements on one epitaxial sample from which the substrate was removed, while Blood [35] has made measurements on two more epitaxial layers. The data of Akita *et al.* [34] and Blood [35] have been limited to the temperature range 300 to 800 K due to evaporation of arsenic. The only electrical measurements made above 900 K on GaAs have been obtained by Roberts [30] and Smith [38]. Roberts' and Smith's measurements were made with a maximum temperature between 1000 and 1190°C on bulk grown crystals in an arsenic atmosphere. In addition, all of these measurements have been analyzed using a Γ -X-L ordering of the conduction band minima.

In this section, electrical measurements are reported in the range 300-1250 K on epitaxial GaAs from which the substrate has been removed by mechanical-chemical polishing. The epitaxial layers have room temperature

carrier concentrations ranging from 10^{15} to 10^{17}cm^{-3} .

In Section 2.1.1 the preparation of these layers and details of the measurements are described, while in Section 2.1.2 the data are analyzed using the new Γ -L-X ordering of the conduction band minima.

2.1.1 Experiment

2.1.1.1 Sample Preparation

The epitaxial layers were grown on Cr-doped semi-insulating GaAs substrates in an AsCl_3 -Ga- H_2 vapor phase reactor [39,40]. The substrates had a crystallographic orientation of $\langle 211 \rangle$ Ga to achieve, simultaneously, a high growth rate [41] and high purity [42]. With a background concentration around 10^{14}cm^{-3} , the doping of the epitaxial layers was controlled by the addition of tin to the gallium melt. In this manner, the epitaxial layers were grown to a thickness of between 280 and 360 μm with doping concentrations in the 10^{15} - 10^{17}cm^{-3} range. The as-grown crystals were cleaved into diamond-shaped samples with areas of about 1cm^2 . The samples were then mounted face down on a lapping block and five μm alumina was used to remove the substrate to within approximately 100 μm of the epitaxial layer. The remaining substrate was then removed with a mechanical-chemical polish using 1% bromine-methanol. This polishing was continued 10 to 20 μm into the epitaxial layer to eliminate any interfacial regions.

To prevent the evaporation of arsenic at high temperatures, the epitaxial layers were encapsulated. The samples were first etched in $\text{H}_2\text{SO}_4:\text{H}_2\text{O}_2:\text{H}_2\text{O}(5:1:1)$ to remove approximately 10 microns, then Si_3N_4 was deposited in a pyrolytic reactor [43] to a thickness of 3000 Å. This Si_3N_4 encapsulation worked well below 1150 K. Above this temperature, however, the Si_3N_4 cracked causing a loss of arsenic. To prevent this, a composite layer of arsenic-doped SiO_2 and Si_3N_4 first described by Lindow *et al.* [44] was used. First 1000 Å of pyrolytic Si_3N_4 was deposited; then approximately 1 μm of arsenic-doped SiO_2 was pyrolytically deposited on top of the Si_3N_4 . This layer maintained its integrity up to 1254 K, which was the maximum temperature used in our measurements. Mask integrity was confirmed when Hall and resistivity measurements with increasing temperature were the same (within experimental error) as with decreasing temperature and subsequent high temperature measurements. Contact windows with a total area of about $1/16 \text{ cm}^2$ were provided by masking growth of the encapsulating material on the four corners of the upper surface.

2.1.1.2 Measurement Apparatus

The apparatus shown in Figure 2.1 was used for the high-temperature resistivity and Hall measurements. To regulate the temperature this apparatus was placed inside an open-tube, two-zone resistance furnace. The furnace

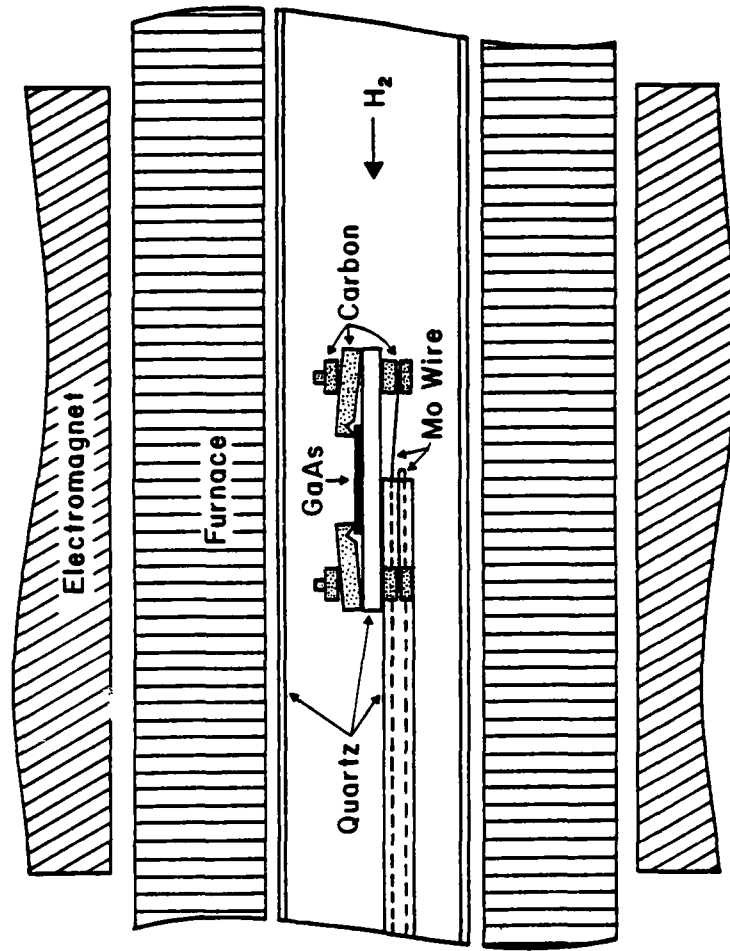


Figure 2.1 Schematic of apparatus used for high-temperature resistivity and Hall measurements.

tube and the silica portions of the apparatus were made of high-purity quartz. The windings of the furnace were made of platinum with an outer casing of aluminum to minimize distortion of the magnetic field. The magnetic field was provided by placing the furnace between the poles of a 4-inch electromagnet. The magnetic field for all measurements was set at 3.5 kG and was measured with a gaussmeter to be within 5% of this value over the 4 inches of the furnace inside the poles of the magnet. Hydrogen, purified with a palladium diffusion cell, was used as the ambient gas to prevent oxidation of the sample or probing apparatus. The temperature was measured with a platinum-10% rhodium thermocouple which, with a digital thermometer, provided an accuracy of $\pm 0.4^{\circ}\text{C}$. The probing apparatus was centered in a two-inch region of constant ($\pm 0.4^{\circ}\text{C}$) temperature which had been centered in the magnetic field.

Above 650 K the carbon probes shown in Figure 2.1 were used to provide ohmic contacts for the resistivity and Hall measurements. The carbon probes were pressure contacts with a sharp edge for contacting the GaAs surface. These probes were held rigid by carbon nuts and screws mounted through a quartz base plate which isolated the four contacts. This plate was mounted on a four-bore quartz capillary tube to provide insulated electrical paths outside the high-temperature zone. High purity molybdenum wire was inserted in the capillaries of the

tubing and connected to the carbon probes by a pressure contact provided by another carbon nut on the carbon screw. The 15-mil diameter molybdenum wire was connected outside the furnace to a switching network arranged to perform van der Pauw measurements. To prevent diffusion of gases through the capillaries of the tubing, the low temperature end was sealed.

Below 650 K the carbon probes give rectifying rather than ohmic contacts. To provide an ohmic contact at these temperatures, a AuSn eutectic alloy was electroplated in the windows of the encapsulant and alloyed at 450°C in a reducing atmosphere. This produced ohmic contacts with the carbon probes from 300 to 650 K.

2.1.1.3 Experimental Results

Several properties of the measured samples are summarized in Table 2.1. The 300 K carrier concentrations were determined from the measured Hall coefficient assuming a Hall factor of unity. The total impurity concentrations, $N_D + N_A$, were calculated from the 77 K mobility [45] for Samples Number 2 and 3. Since this technique is not valid for heavier-doped samples, similar data were obtained from the 300 K mobility [46] for Sample Number 1.

The resistivity, ρ , was measured by the van der Pauw [47] technique. All the samples had a resistance ratio between 1.05 and 1.00 in both the low (300-600 K) and high (650-1250 K) temperature ranges. This ratio was also temperature

Table 2.1 Sample Properties

Sample No.	n_{300K} (cm^{-3})	$N_D + N_A$ (cm^{-3})	$\frac{N_A}{N_D}$	Thickness (μm)
1	1.2×10^{17}	2.0×10^{17}	0.25	340
2	9.7×10^{15}	1.6×10^{16}	0.23	310
3	1.9×10^{15}	4.2×10^{15}	0.38	260

independent. The resistances were calculated from the slope of the current-voltage characteristics by linear regression. These characteristics were obtained from voltage measurements for at least three different currents for each measurement. The voltage was measured using a high impedance digital multimeter to four digit accuracy, while the current was supplied by a constant current source. The measured I-V characteristics were linear: that is, the coefficient for determination of linear regression was 0.9999 ± 0.0001 , while an optimum fit would be 1.0. The resistivity showed the expected increase from the room temperature value with rising temperature due to increased scattering of the carriers. As intrinsic conduction began to dominate, the resistivity started decreasing with increasing temperature due to the increase in the carrier concentration.

The Hall coefficient, R_H , was measured in a magnetic field of 3.5 kG with the van der Pauw [47] technique. Since the samples were diamond-shaped, the current was directed through the longest path to give the best accuracy. We estimate the cumulative errors of the measurements under these conditions to be under 5%. The single-band carrier concentration was calculated from the Hall coefficient by,

$$n = \frac{1}{qR_H} ,$$

where q is the electronic charge, and the Hall scattering factor was assumed to be unity. This assumption introduces a small temperature-dependent error in the analysis [48]. The temperature dependencies of this single-band carrier concentration for the samples indicated in Table 2.1 are plotted in Figure 2.2. Since all the donors are thermally ionized at room temperature, the carrier concentration remains constant until sufficient carriers are thermally excited into higher conduction band minima. The slight apparent rise in the carrier concentration up to 400 K is due to the decrease in the Hall factor for polar mode scattering [48]. As the samples are heated into the 600 K range, there is a noticeable rise in the Hall coefficient due to the thermal excitation of carriers into the lower mobility L_6^C minima. The sharp rise of the single-band carrier concentration above 750 K for the highest-doped sample is due to the onset of intrinsic conduction. This is confirmed by the higher temperatures needed to produce equivalent increases for the heavier-doped samples.

The measured mobility, μ_m , is determined as the Hall coefficient divided by the resistivity: R_H/ρ . These mobility values for the temperature range 300-1250 K are plotted in Figure 2.3. The mobility variations of the lighter-doped samples have characteristics similar to the samples measured by Blood [35].

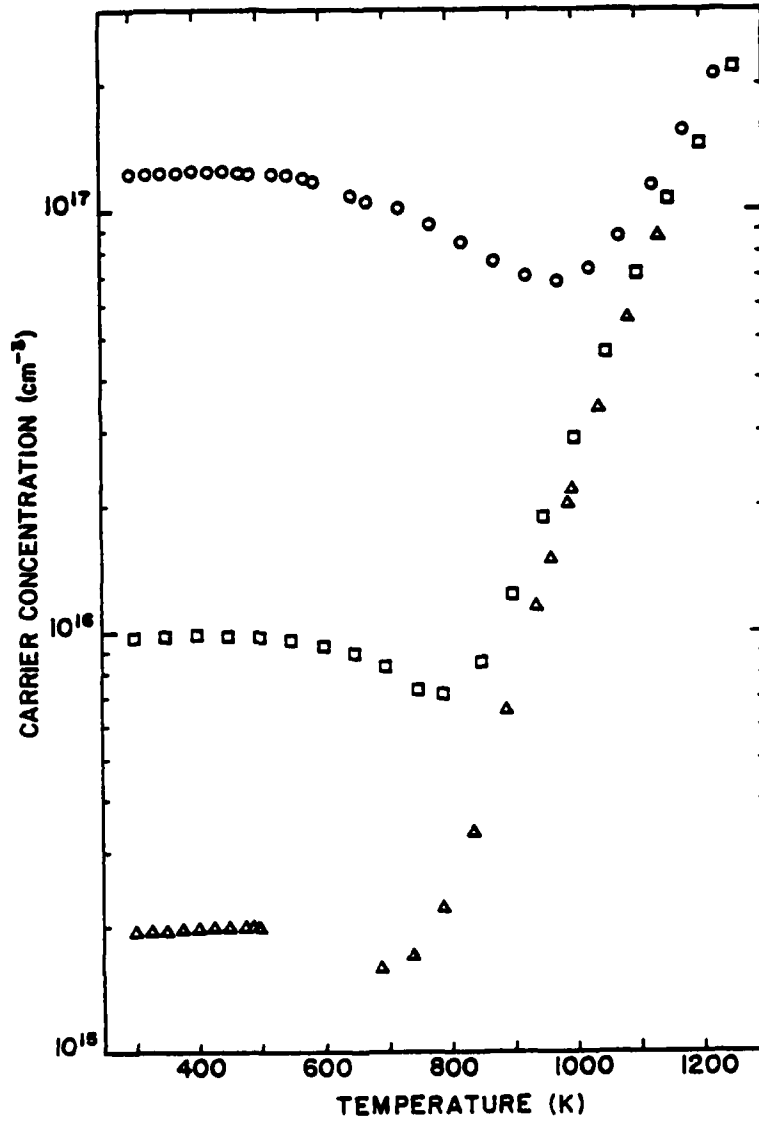


Figure 2.2 Reciprocal of Hall coefficient times the elementary charge as a function of temperature for three GaAs epitaxial samples.

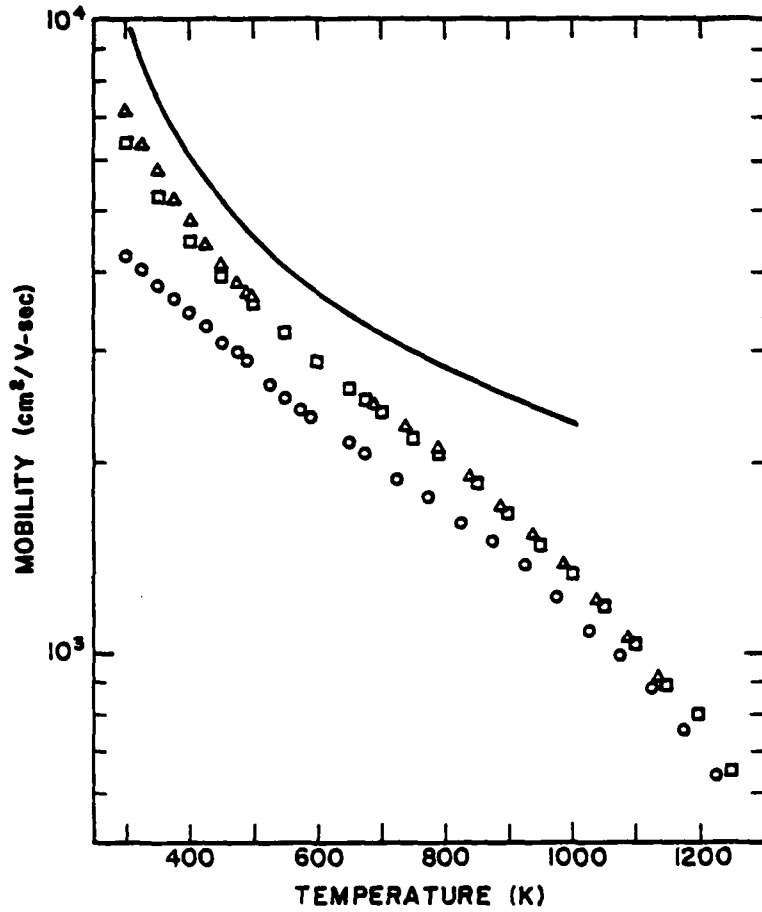


Figure 2.3 Measured mobility, R_H/ρ , versus temperature for three GaAs epitaxial samples. The solid line is from the analysis by Rode [49,50].

In the range 300-500 K the mobility can be expressed as $\mu_m \propto T^{-N}$ with $N = 1.25$, while in the range 500-700 K the temperature dependence is slower. Above 750 K the measured mobility values for the lighter-doped samples again fall rapidly with temperature. These variations with temperature are similar to those calculated by Rode [49,50] for pure GaAs. In comparison, however, our samples have a slightly reduced slope between 300 and 500 K due to ionized impurity scattering [51]. Thus, the $9.7 \times 10^{15} \text{ cm}^{-3}$ doped Sample Number 2 has a smaller slope than the $1.9 \times 10^{15} \text{ cm}^{-3}$ doped Sample Number 3.

Above 500 K the slope of the data for the lighter-doped samples decreases. This feature is predicted by Rode's analysis [49,50]. However, the calculation does not account for the increase in slope above 750 K. This behavior can be partially ascribed to thermal transfer of electrons from the high mobility Γ_6^C minimum to the low mobility L_6^C minima [50]. The heaviest doped Sample Number 1, however, does not show this decrease at 750 K, but rather at 950 K. This is partially due to the high ionized-impurity scattering of Sample Number 1, combined with the fact that, when intrinsic conduction dominates, a different scattering mechanism begins to cause a rapid decrease of the mobility in the Γ_6^C minimum. This mechanism is the scattering of carriers from the Γ_6^C minimum to the L_6^C minima, then back to the Γ_6^C minimum [52]. It is obvious

that this mechanism is strongly dependent on the number of carriers in the upper portion of the Γ_6^C minimum. Therefore, both temperature and carrier concentration are important factors. The combined effect of this scattering mechanism and the thermal transfer to lower-mobility upper minima determines the mobility at high temperature. Thus, above 1100 K the measured mobility data for all of the samples begin to approach the same value.

To summarize the findings of this section, we find good agreement among our experimental temperature dependence of the measured mobility, Blood's experimental data, and Rode's calculations.

2.1.2 Analysis

2.1.2.1 Energy Separations

In contrast to previous conduction-band ordering in GaAs, Aspnes *et al.* [53] have recently found, from Schottky barrier electroreflectance measurements, that the L_6^C conduction band minima are 170 ± 30 meV below the X_6^C minima. Aspnes [54,55] has also shown that all present experimental data can be reinterpreted using $\Gamma_6^C-L_6^C-X_6^C$ ordering of the conduction band minima. The temperature dependence of these minima with respect to the valence band is needed to determine the intrinsic carrier concentration and relative occupancy of various minima at high temperatures. The top of the valence band, Γ_8^V , will be used as the reference energy ($E=0$) throughout the following discussion.

The $\Gamma_6^C - \Gamma_8^V$ separation has been measured with great accuracy by Sell *et al.* [56,57] and by Panish and Casey [58]. These data were used by Thurmond [59] to determine the coefficients E_0 , α , and β of the equation given by Varshni [60],

$$E_{\Gamma} = E_{\Gamma_0} - \alpha T^2 / (T + \beta), \quad (2.1)$$

as 1.519 eV, 5.405×10^{-4} eV/K, and 204 K, respectively. These coefficients predict energies that agree with experiment with a mean-square deviation of 2.6 meV.

The $X_6^C - \Gamma_8^V$ separation can be determined from the above data and data on indirect transitions from the electrons. at Γ_6^C to higher conduction band minima in degenerate n-type material. Using the data of Onton [61], Aspnes determined the $X_6^C - \Gamma_6^C$ separation by lineshape analysis to be 0.462 ± 0.005 eV at 2 K. This results in a separation of 1.981 eV at 2 K. The coefficient β in Equation (2.1) is related to the Debye temperature for the fundamental absorption edges of Si, Ge, GaP and GaAs [54]. From data for Si and GaP, Aspnes assumes that $\beta = 204$ K for the $X_6^C - \Gamma_8^V$ separation in GaAs. By analyzing transport data and combining the results with a rigid-band hypothesis [62] and results of measurements on GaP [63], Aspnes [54] calculates the α coefficient of Equation (2.1) for X_6^C to be 4.6×10^{-4} eV/K.

The $X_6^C - L_6^C$ energy separation has been determined from core-level electroreflectance measurements to be 0.17 ± 0.03 eV at 110 K [53]. To determine the coefficient α for

Table 2.2 Energies and temperature dependence of the Γ_6^C , L_6^C and X_6^C conduction-band minima of GaAs relative to the top of the valence band, Γ_8^V . The coefficients E_0 , α and β are defined by Equation 2.1.

	E_0 (eV)	α (eV/K)	β (K)
Γ_6^C	1.519	5.405×10^{-4}	204
L_6^C	1.818	6.5×10^{-4}	204
X_6^C	1.981	4.6×10^{-4}	204

the $L_6^C-\Gamma_8^V$ separation Aspnes [54] uses the Auvergne *et al.* [62] postulate of rigid valence bands and his measured energy shift of 115 meV of the $L_6^C-L_6^V$ transition from 4 to 295 K from Schottky barrier electroreflectance measurements in the 3 eV range [64]. From this he calculates $\alpha = 6.5 \times 10^{-4}$ eV/K for the $L_6^C-\Gamma_8^V$ separation [54]. Using this α and the $X_6^C-L_6^C$ energy separation at 110 K, the $L_6^C-\Gamma_8^V$ separation at 0 K is calculated to be 1.818 eV. All of the coefficients for the temperature dependencies of the valence band-to-conduction band energies are summarized in Table 2.2.

2.1.2.2 Four-Band Model

To calculate the true carrier concentration a four-band model is needed. The Hall coefficient under these conditions is

$$R_H = \frac{n_\Gamma \mu_\Gamma^2 + n_L \mu_L^2 + n_X \mu_X^2 - p \mu_h^2}{q(n_\Gamma \mu_\Gamma + n_L \mu_L + n_X \mu_X - p \mu_h)^2}, \quad (2.2)$$

where n_Γ , n_L and n_X are the electron concentrations; μ_Γ , μ_L and μ_X are the electron mobilities; p is the hole concentration; and μ is the hole mobility in the valence band maxima. The corresponding expression for the resistivity is

$$\rho = \frac{1}{q(n_\Gamma \mu_\Gamma + n_L \mu_L + n_X \mu_X + p \mu_h)}. \quad (2.3)$$

To eliminate two unknowns in these equations the relative occupancy of the conduction band minima can be calculated for nondegenerate material using Boltzman statistics. Although Sample Number 1, with a doping level of $1.2 \times 10^{17} \text{ cm}^{-3}$ is degenerate at room temperature, beyond 450 K (the temperature range of interest) it is non-degenerate. Defining $n_L/n_\Gamma \equiv a$ and $n_X/n_\Gamma \equiv b$, the relative occupancy can be expressed as,

$$a = \left\{ \frac{m_L}{m_\Gamma} \right\}^{3/2} \exp \left\{ \frac{E_\Gamma - E_L}{kT} \right\}, \text{ and} \quad (2.4)$$
$$b = \left\{ \frac{m_X}{m_\Gamma} \right\}^{3/2} \exp \left\{ \frac{E_\Gamma - E_X}{kT} \right\},$$

where E_Γ , E_L , and E_X are the respective separations between the various minima and Γ_8^V . m_Γ , m_L and m_X are the respective effective masses of the minima.

2.1.2.3 Effective Masses

For a parabolic band the density-of-states mass can be expressed as

$$m_\xi = \left\{ N_\xi m_{t_\xi} m_{l_\xi}^{1/2} \right\}^{2/3}, \quad (2.5)$$

where m_{t_ξ} and m_{l_ξ} are the transverse and longitudinal masses, and N_ξ is the number of equivalent minima. The isotropic Γ_6^C mass, m_Γ , at 2 K is $m_{t_\Gamma} = m_{l_\Gamma} = 0.0665m$ [65]. The variation of this mass with temperature can be

calculated from $\vec{k} \cdot \vec{p}$ theory [66] according to

$$\frac{m_{\Gamma}}{m} = \frac{1}{1 + E_P \left\{ \frac{2}{E_{\Gamma}} + \frac{1}{E_{\Gamma} + \Delta} \right\}}, \quad (2.6)$$

where E_P is an energy related to the momentum matrix element, and $\Delta = 0.341$ eV is the spin-orbit splitting, $\Gamma_8^V - \Gamma_7^V$ [64]. From the temperature dependence of the Γ energy gap and the above data, E_P is calculated to be 7.51 eV. Thus, using Equation (2.6) the temperature dependence of the effective mass in the Γ_6^C minimum is

$$\frac{m_{\Gamma}}{m} = \frac{1}{1 + 7.51 \left\{ \frac{2}{E_{\Gamma}} + \frac{1}{E_{\Gamma} + 0.341} \right\}}. \quad (2.7)$$

where the temperature dependence of E_{Γ} is given by Equation (2.1).

Aspnes [54] calculates the transverse effective mass for the L_6^C minima from his Schottky barrier electroreflectance measurements [64] to be 0.0754m. He estimates the longitudinal mass at L_6^C by comparison of GaAs with Ge. His estimated longitudinal mass value of 1.9m leads to a density-of-states effective mass of $m_L = 0.56m$ at 0 K [54]. The temperature dependence of this density-of-states effective mass is determined by the temperature variation of the $L_6^C - L_6^V$ interband energy separation which affects the transverse mass, m_{t_L} [54]. Using Equation (2.5), the data

of Table 2.1, $\vec{k} \cdot \vec{p}$ theory and the values calculated by Aspnes, the density-of-states effective mass for the L_6^C minima as a function of temperature can be expressed as

$$\frac{m_L}{m} = \{5.51 [1 + 19.3 (\frac{1}{E_1(\text{ev})} + \frac{1}{E_1(\text{ev}) + 0.22})]\}^{2/3} \quad (2.8)$$

where E_1 is the $L_6^C-L_6^V$ interband energy separation.

We use the X_6^C density-of-states effective mass of 0.85m calculated by Pitt and Lees [67] from their high-pressure Hall effect and resistivity data. No temperature dependence is assumed for the effective mass at X_6^C . This is a reasonable assumption since even at 1250 K we estimate the percentage of carriers in the X_6^C minima to be at most only 5%.

2.1.2.4 Hall Coefficient

2.1.2.4.1 Extrinsic Conductivity

If the material has a carrier concentration well above the intrinsic concentration, then the contribution of the holes can be neglected. Below 1000 K the carriers in the X_6^C minima represent less than 3% of the total number of carriers in the conduction bands. Since the mobility of the carriers in the X_6^C minima is the lowest of the conduction band minima at Γ , L, and X, the total effect of the carriers in X_6^C can be neglected for the Hall coefficient [Equation (2.2)] and resistivity equations [Equation (2.3)].

Neglecting the carriers in the Γ_8^V maxima and X_6^C minima, the expression for the Hall coefficient from Equation (2.2) becomes

$$q R_H = \frac{1 + a\beta^2}{n_\Gamma (1+a\beta)^2}, \quad (2.9)$$

where a is defined by Equation (2.4) and $\beta = \mu_L/\mu_\Gamma$.

Using the temperature dependence of the energy gaps given in Table 2.2 and the effective masses given in Equations (2.7) and (2.8), a can be calculated. Combining this value of a and the measured Hall coefficient into Equation (2.9) yields an equation that has two unknowns: n_Γ and β . Another equation can be obtained if the total concentration of the layer is assumed to be the doping concentration, $N_D - N_A$. This is a valid assumption since there are no appreciable deep donor levels and the intrinsic concentration is small enough to neglect. Thus, it is assumed that

$$n_\Gamma + n_L = n_{400 K}. \quad (2.10)$$

The 400 K carrier concentration was chosen because the Hall factor for polar mode scattering is a minimum at this temperature

Combining Equations (2.9) and (2.10) yields the equation,

$$q R_H = \frac{(1+a) (1+a\beta^2)}{n_{400K} (1+a\beta)^2} , \quad (2.11)$$

which has only one unknown: β . This mobility ratio, β , was calculated for the heavier-doped Samples Number 2 and 3. The results for these epitaxial layers are plotted in Figure 2.4. The measurements were done until intrinsic conduction could no longer be neglected in Equation (2.9). The final point calculated for Sample Number 1 used a modified Equation (2.10). That is, the intrinsic carrier concentration was added to the 400 K concentration in Equation (2.10). However, because of the small mobility of holes, the intrinsic conduction can still be neglected in Equation (2.9). The temperature dependence shown in Figure 2.4 indicates that the assumption of a constant mobility ratio for samples doped above 10^{16} cm^{-3} is a poor assumption. It will be shown later in this paper that the results in Figure 2.4 also apply to Sample Number 3 doped at $1.9 \times 10^{15} \text{ cm}^{-3}$.

For pure GaAs intravalley polar-optical scattering predominates in the Γ_6^C conduction band minimum [50] until intrinsic conduction becomes predominant. Even the purest samples measured by Blood [35] and our Sample Number 3

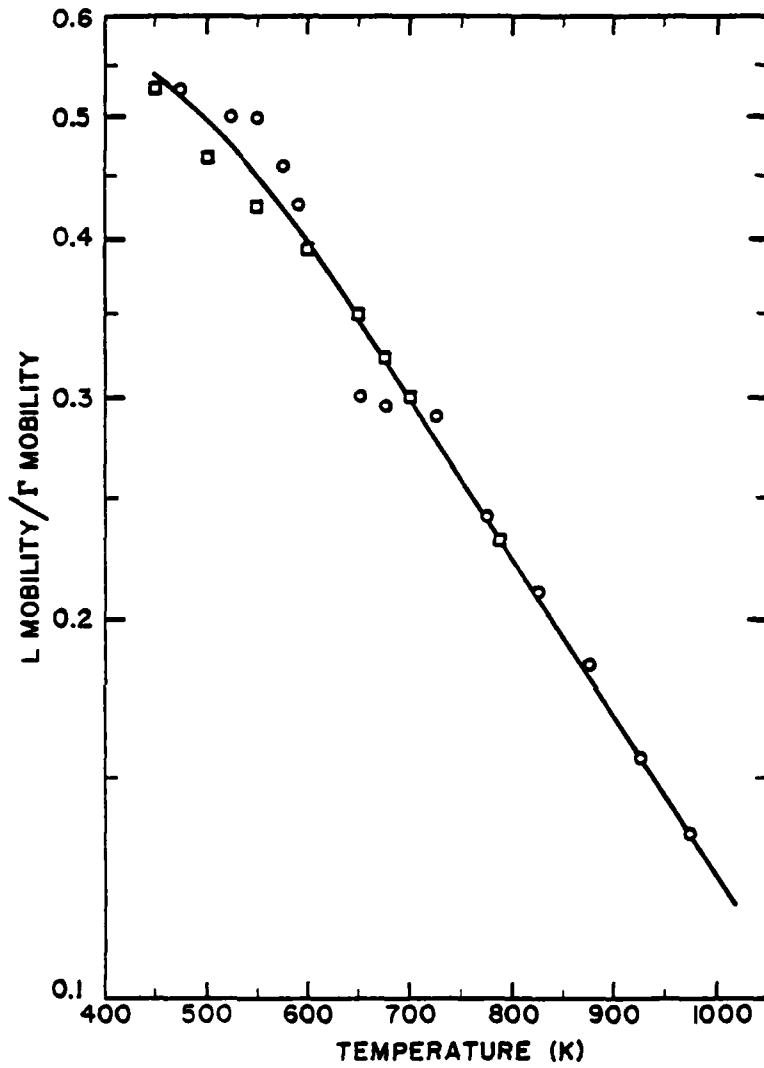


Figure 2.4 Ratio of the mobility in the L_6^C minima to the mobility in the Γ_6^C minimum as a function of temperature for Samples No. 1 (○) and No. 2 (□).

show a smaller temperature dependence [49] between 300-500 K than would be expected for pure GaAs. This is due to ionized-impurity scattering, which will be important for the mobility of the carriers in Γ_6^C . However, it will have a much smaller effect on the carriers in L_6^C . The dominant scattering mechanism in the X_6^C minima is equivalent intervalley scattering [68,69] and this mechanism can likewise be assumed to dominate the mobility in the L_6^C minima. Although scattering between equivalent valleys leads to a larger temperature coefficient than measured in our samples [70], in GaP the observed value [71] is not significantly different from that of Γ_6^C . If the same applies to GaAs, then for pure GaAs the mobility ratio, β , will remain constant with increasing temperature. However, ionized impurity scattering reduces the temperature dependence of the Γ_6^C minimum, causing the observed temperature dependence of the mobility ratio, β , given in Figure 4.

2.1.2.4.2 Intrinsic Conductivity

Near the point where intrinsic conduction begins to become important, the ratio of the hole mobility to the electron mobility in Γ_6^C can be calculated. This was done by using the intrinsic mass action law,

$$(n_{\Gamma} + n_L)p = n_i^2, \quad (2.12)$$

obtained by neglecting the contributions of the carriers in

the X_6^C minima. The previous Equations (2.9) and (2.10) become,

$$q R_H = \frac{1+a\beta^2 - \left[\frac{p}{n_\Gamma}\right] \left[\frac{\mu_h}{\mu_\Gamma}\right]^2}{n_\Gamma \left\{ 1 + a\beta - \left[\frac{p}{n_\Gamma}\right] \left[\frac{\mu_h}{\mu_\Gamma}\right] \right\}^2}, \text{ and} \quad (2.13)$$

$$n_\Gamma + n_L = n_{400K} + n_i.$$

Using the energy gap parameters in Table 2.2 and the effective masses given in Equations (2.7) and (2.8), the intrinsic carrier concentration was calculated. This intrinsic concentration was used in Equations (2.12) and (2.13) and the mobility ratio μ_h/μ_Γ was calculated in the 900-1000 K range for Sample Number 1 and in the 750-850 K range for Sample Number 2. It was found that this ratio was approximately 0.053, which is the same as the room temperature value. Thus, the ratio μ_h/μ_Γ was assumed to be constant.

2.1.2.5 Resistivity

Neglecting the contribution of the holes and the electrons in X_6^6 , Equation (2.3) becomes,

$$\rho = \frac{1}{q\mu_\Gamma(n_\Gamma + n_L\beta)}. \quad (2.14)$$

With this equation, the β calculated in Figure 2.4, the measured resistivity, and Equations (2.4) and (2.10), the

mobilities μ_{Γ} and μ_L were calculated. These mobilities are plotted versus temperature in Figure 2.5, along with the hole mobility.

With these mobilities a three-band carrier concentration can be calculated. To calculate the desired four-band carrier concentration an assumption must be made about the temperature dependence of the X_6^C mobility. We have assumed that the X_6^C mobility is one-third the L_6^C mobility, based on the higher density of states at X_6^C and high pressure transport measurements [54]. We have also assumed that the X_6^C and L_6^C mobilities have the same temperature dependence, since intravalley scattering dominates the mobility for both sets of minima. Using these assumptions and the mobilities in Figure 2.5, the four-band carrier concentration was calculated from Equations (2.1), (2.2), (2.4), (2.7), (2.8), and the data in Table 2.2. When intrinsic conduction begins to dominate as previously discussed, intervalley scattering between Γ_6^C and L_6^C begins to control the Γ_6^C mobility. This causes the mobility ratio, β , to flatten out or to start increasing [52]. Under extrinsic conditions the best results for the four-band carrier concentration were obtained when the mobility ratio, β , was taken to have the value in Figure 2.4. When Sample Numbers 1, 2, and 3 reached 1050, 950, and 900 K, respectively, the mobility ratio leveled off and began to rise

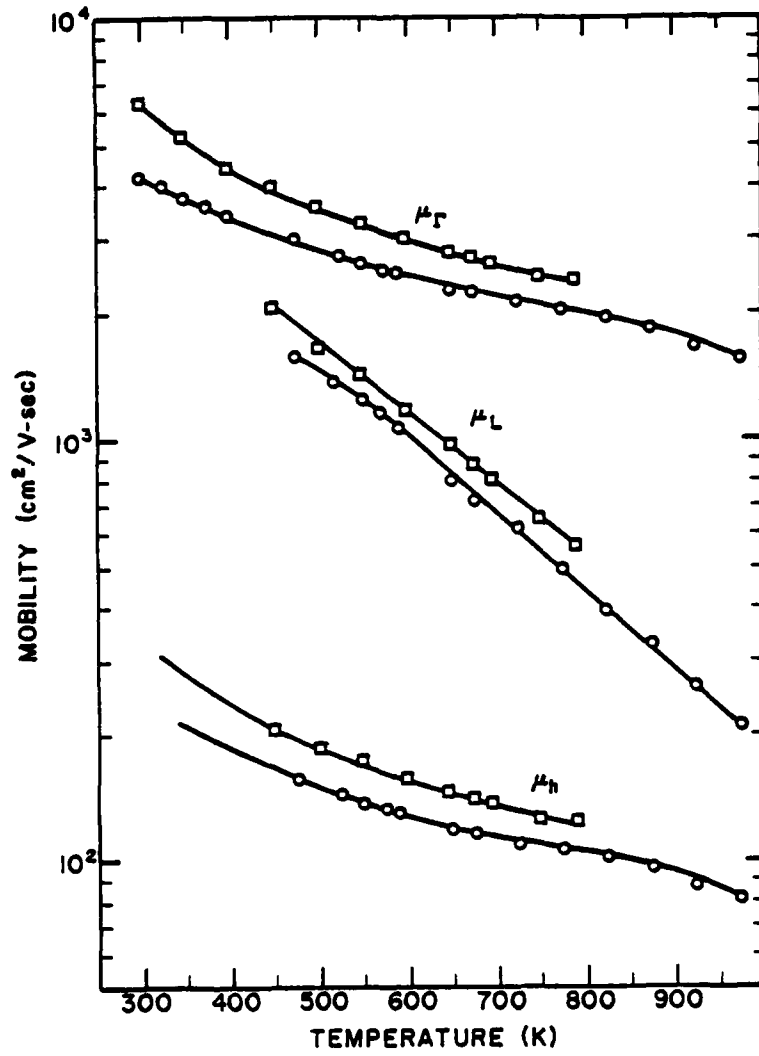


Figure 2.5 Mobilities in the Γ_6^C minimum, L_6^C minima and Γ_8^V maxima as a function of temperature for Samples No. 1 (○) and No. 2 (□).

slightly. This rise was approximately 5% for every 100 K increase in temperature. The final four-band carrier concentration versus temperature is plotted in Figure 2.6. The calculated intrinsic carrier concentration was calculated using the data in Table 2.2 and Equations (2.1), (2.7) and (2.8).

2.1.3 Conclusions

From the preceding results and the other data discussed, a self-consistent model has been developed for the evaluation of carrier transport in n-type GaAs at elevated temperatures. This model supports the $\Gamma_6^C-L_6^C-X_6^C$ ordering of the conduction-band minima demonstrated by Aspnes and co-workers. The temperature dependencies of the various energy separations have been shown, within experimental error, to have the variations given in Table 2.2.

Using these temperature dependencies of the energy separations and the effective mass variations, a four-band intrinsic carrier concentration has been calculated which is consistent with measured data at high temperatures. We, therefore, expect this calculated intrinsic carrier concentration to be correct within experimental error.

The temperature dependence of the mobility in the L_6^C minima was shown to decrease faster with increasing

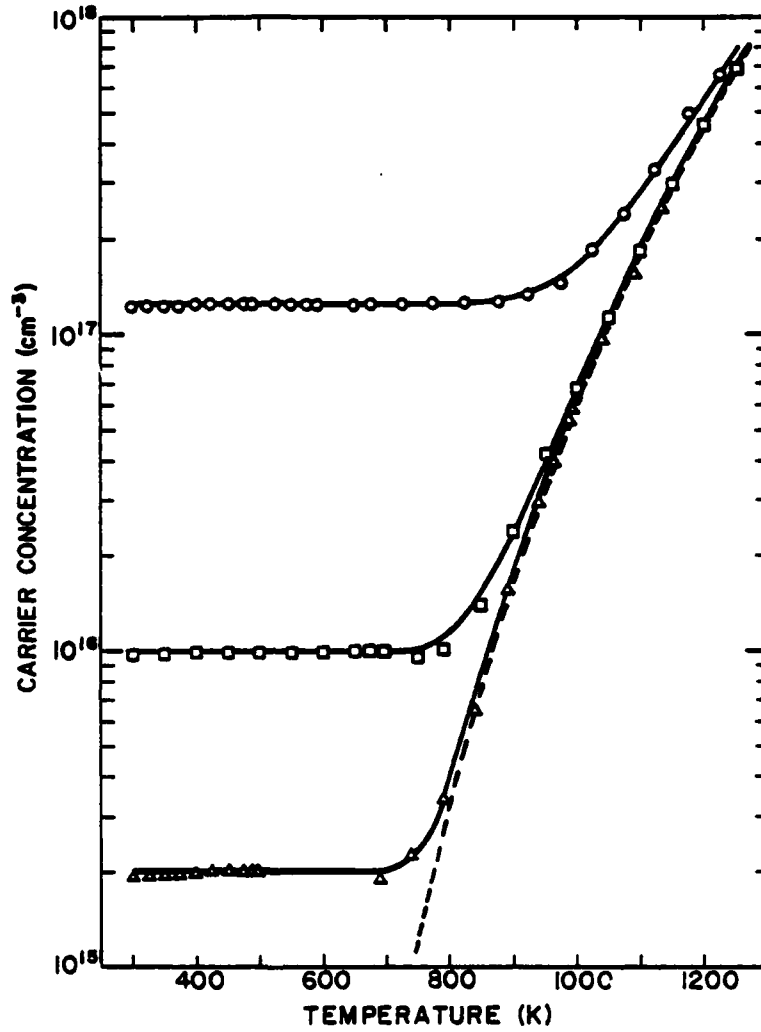


Figure 2.6 Four-band carrier concentration as a function of temperature for GaAs epitaxial Samples No. 1 (○), No. 2 (□) and No. 3 (△). The dashed line is the calculated intrinsic carrier concentration.

temperature than the mobility in the Γ_6^C minimum. This different temperature dependence is attributed to different scattering mechanisms. In the L_6^C minima equivalent intervalley scattering dominates the mobility, while in Γ_6^C a combination of polar-mode and ionized-impurity intravalley scattering dominates. Therefore, taking the ratio of the mobility in L_6^C to the mobility in Γ_6^C as constant is not applicable to layers doped above 10^{15} cm^{-3} . When intrinsic conduction dominates, intervalley scattering between Γ_6^C and L_6^C will cause the mobility in Γ_6^C to have a slightly greater temperature dependence than the mobility in L_6^C .

Combining the temperature dependence of the mobilities and energy gaps with the four-band Hall coefficient equation produced results which were consistent with the calculated intrinsic carrier concentration and the measured carrier concentration.

2.2 SUBSTRATES

To model epitaxial growth phenomena the carrier concentrations of the substrates at high temperature must be known. Thus, high-temperature Hall measurements were performed on both heavily-doped and chromium-doped substrates. The substrates were prepared using the encapsulation procedure of Section 2.1.1.1. The measurement apparatus was exactly the same as described in

Section 2.1.1.2, however, no measurements were made below 650 K.

The resistivity, ρ , was measured by the van der Pauw technique [47]. All the samples had a resistance ratio between 1.05 and 1.00 which was temperature independent. The resistances were calculated from the slope of the current-voltage characteristics by linear regression. These characteristics were obtained from voltage measurements for at least three different currents for each measurement. The voltage was measured using a high impedance digital multimeter to four digit accuracy, while the current was supplied by a constant current source. The measured I-V characteristics were linear: that is, the coefficient for determination of linear regression was 0.9999 ± 0.0001 , while an optimum fit would be 1.0.

The Hall coefficient, R_H , was measured in a magnetic field of 3.5 kG with the van der Pauw technique [47]. Since some of the samples were diamond-shaped, the current was directed through the longest path to give the best accuracy. The single-band carrier concentration was calculated from the Hall coefficient by,

$$n = \frac{1}{qR_H} ,$$

where q is the electronic charge, and the Hall scattering factor was assumed to be unity. This assumption introduces a small

temperature-dependent error in the analysis [48]. The temperature dependencies of this single-band carrier concentration for the chromium-doped substrates are plotted in Figure 2.7.

The measured mobility, μ_m , is determined as the Hall coefficient divided by the resistivity: R_H/ρ . These mobility values for the temperature range 650-1225 K are plotted in Figure 2.8. The range of mobility values from approximately $2000 \text{ cm}^2/\text{V-sec}$ at 650 K to $700 \text{ cm}^2/\text{V-sec}$ at 1200 K is the same range exhibited by the heaviest doped sample in Figure 2.3. This similarity indicates that there is a large amount of ionized impurity scattering in the chromium-doped substrates.

The data in Figure 2.7 and the Hall measurements of a heavily-doped substrate at 1000 K were interpreted using the four-band model developed in Section 2.1. The multi-band electron concentrations for the chromium-doped substrates as a function of temperature are shown in Figure 2.9. The dashed line is the calculated intrinsic carrier concentration. From these data, below 1100 K the chromium-doped substrates are slightly p-type, while above 1100 K they appear to be intrinsic. This indicates that these substrates do not have the pinned Fermi level observed by Zucca [36].

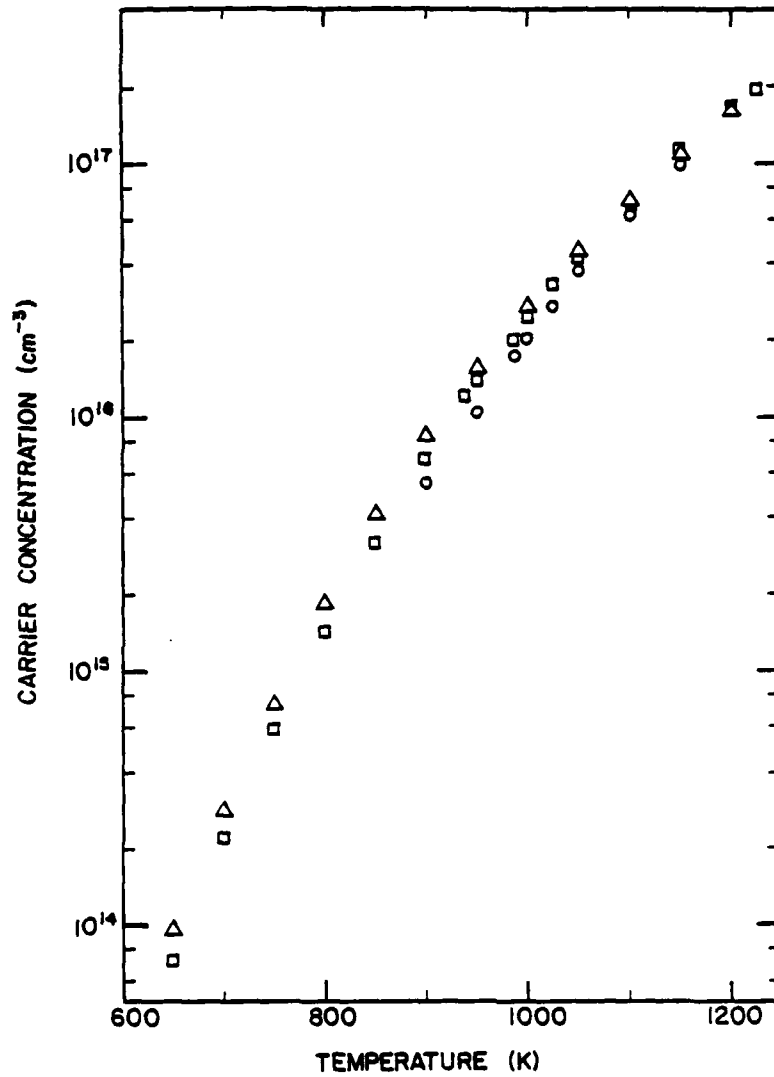


Figure 2.7 Reciprocal of Hall coefficient times the elementary charge as a function of temperature for three Cr-doped GaAs substrates.

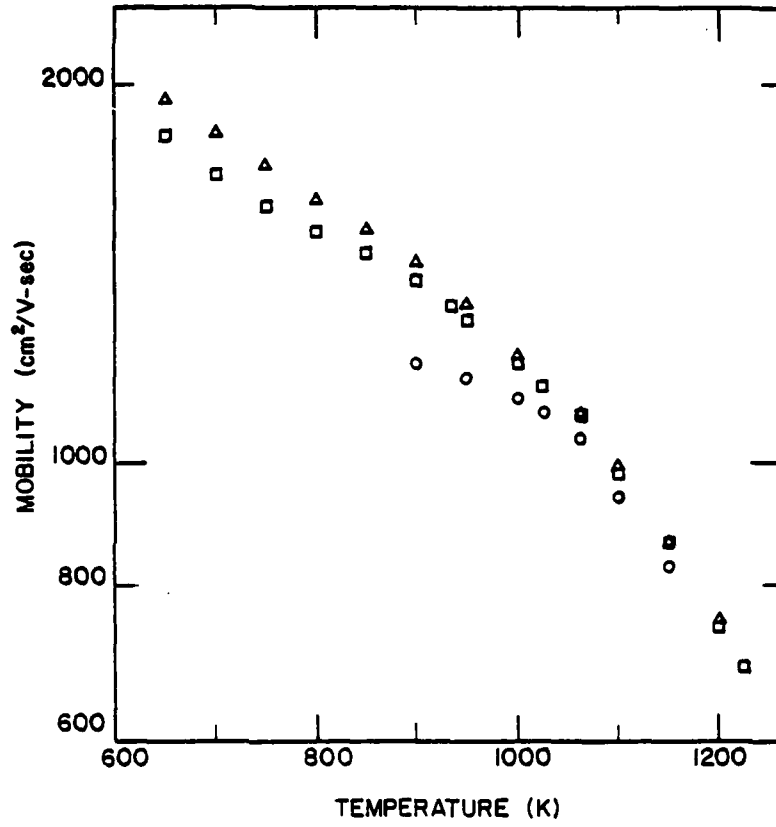


Figure 2.8 Measured mobility, R_H/ρ , versus temperature for three Cr-doped GaAs substrates.

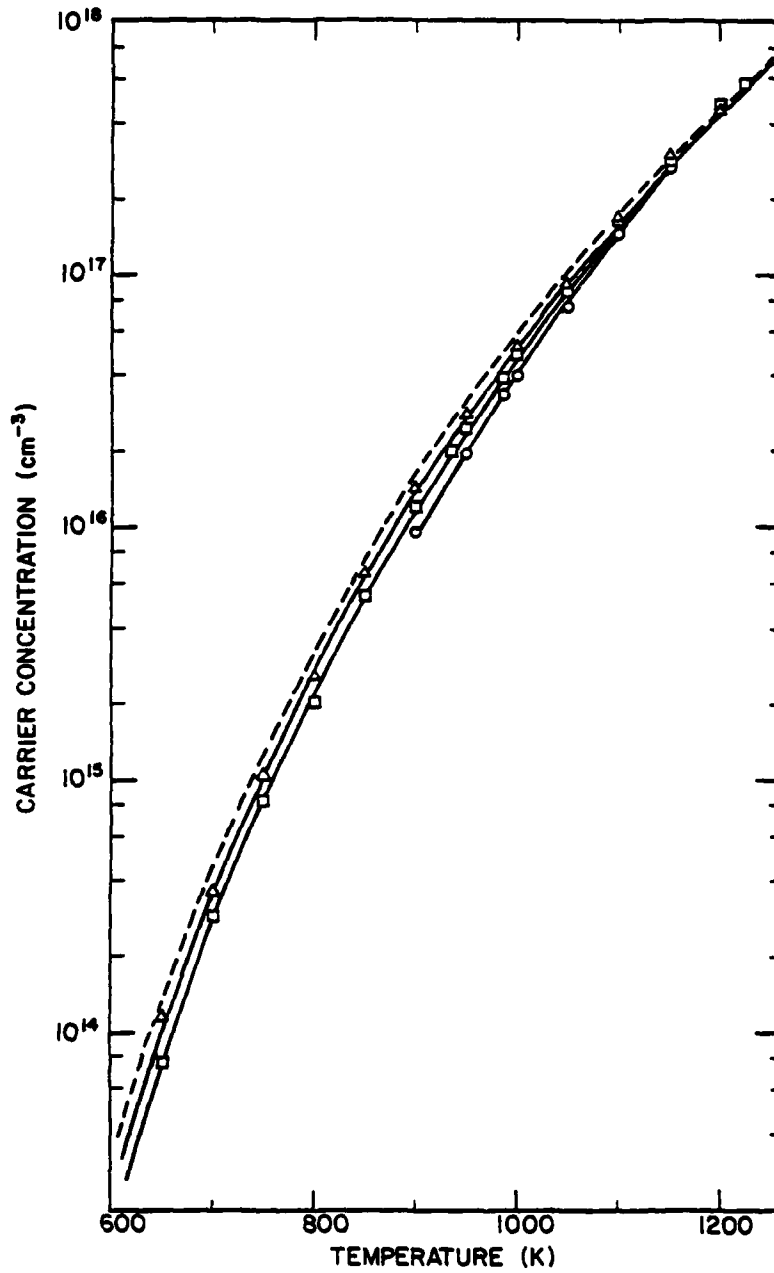


Figure 2.9 Four-band electron concentration as a function of temperature for three Cr-doped GaAs substrates. The dashed line is the calculated intrinsic carrier concentration.

The heavily-doped substrate was only measured at room temperature and 1000 K. Using the multi-band model, the substrate was still heavily-doped ($1.8 \times 10^{18} \text{cm}^{-3}$) at 1000 K. Thus, as expected a heavily-doped substrate will remain extrinsic until temperatures far exceeding those used for epitaxial growth are reached.

In conclusion, chromium-doped substrates are slightly p-type while heavily-doped substrates are n^+ at the temperatures commonly encountered for vapor-phase epitaxial growth.

3. IMPURITY GRADIENT MODEL

From the high-temperature Hall data of Section 2, it can be seen that the carrier concentrations, at typical growth temperatures, in the substrate and the growing epitaxial layer are different for many commonly-encountered growth situations. The situations presented in Figure 1.4, for the growth of a lightly-doped epitaxial layer on a heavily-doped substrate and the growth of an extrinsic layer on a nearly intrinsic chromium-doped substrate, are two examples where this occurs. Once carrier concentrations in the substrates and the growing layers are known from the high-temperature Hall data, quantitative impurity gradient models can be developed for these and other epitaxial growth situations.

3.1 TIME-DEPENDENT ANALYSIS

3.1.1 Electric Field

For a time-dependent analysis of the problem only two assumptions are required to find a formal solution for the electric field. These assumptions are as follows:

(1) The epitaxial growth rates are small enough that the physical processes are approximately in thermodynamic equilibrium.

(2) Since the donor and acceptor mobilities, μ_d and μ_a , are much less than the electron and hole mobilities,

μ_n and μ_p , it is assumed that the ionized donor and acceptor concentrations, N_d and N_a , are sufficiently small that $N_d \mu_d, N_a \mu_a \ll n \mu_n, p \mu_p$.

With these assumptions the equations to be solved are Poisson's equation,

$$\frac{\partial E}{\partial x} = \frac{q}{\epsilon \epsilon_0} \sum_j N_j, \quad (3.1)$$

where $N_j = +N_d, -N_a, +p, -n$;

the conduction current equations for ionized donors, acceptors, electrons, and holes,

$$J_j = q \mu_j N_j E \mp q D_j \frac{\partial N_j}{\partial x}; \quad (3.2)$$

and the continuity equations,

$$q \frac{\partial N_j}{\partial t} = \mp \frac{\partial J_j}{\partial x}, \quad (3.3)$$

where the upper - sign in the current and continuity equations is for the positively charged donors and holes, while the lower + sign is for the negatively charged acceptors and electrons. At low growth rates, the total current is zero,

$$J = \sum_j J_j + \epsilon \epsilon_0 \frac{\partial E}{\partial t} = 0; \quad (3.4)$$

and for dilute solutions the mass action laws are

$$np = n_i^2, \quad nN_d = K_d N_d^0, \quad pN_a = K_a N_a^0, \quad (3.5)$$

where N_d^0 and N_a^0 are the neutral donors and acceptors, and n_i^2 , K_d and K_a are the equilibrium constants. In these equations N_j , J_j and E are assumed to be functions of time, t , and distance from the substrate, $-x$.

Putting Equation (3.2) into Equation (3.4) produces

$$\begin{aligned} & qE (\mu_d N_d + \mu_a N_a + \mu_p P + \mu_n n) \\ & + q(-D_d \frac{\partial N_d}{\partial x} + D_a \frac{\partial N_a}{\partial x} - D_p \frac{\partial P}{\partial x} + D_n \frac{\partial n}{\partial x}) \\ & + \epsilon \epsilon_0 \frac{\partial E}{\partial t} = 0, \end{aligned} \quad (3.6)$$

which with Assumption 2 and Einstein's relation reduces to

$$E = \frac{kT}{q} \frac{(\mu_p \frac{\partial P}{\partial x} - \mu_n \frac{\partial n}{\partial x})}{(\mu_p P + \mu_n n)} - \frac{\epsilon \epsilon_0 \frac{\partial E}{\partial t}}{q(\mu_p P + \mu_n n)}. \quad (3.7)$$

Using the mass action law for the generation of holes and electrons given in Equation (3.5), Equation (3.7) becomes

$$E = - \frac{kT}{q} \left(\frac{1}{n}\right) \frac{\partial n}{\partial x} - \frac{n \epsilon \epsilon_0}{q(\mu_p n_i^2 + \mu_n n^2)} \frac{\partial E}{\partial t}. \quad (3.8)$$

Equation (3.8) can be rewritten as

$$\frac{\partial E}{\partial t} + \frac{\partial Q}{\partial t} E = - \frac{kT}{q} \left(\frac{1}{n}\right) \frac{\partial n}{\partial x} \frac{\partial Q}{\partial t}, \quad (3.9)$$

where

$$Q = \frac{q}{\epsilon \epsilon_0} \int_0^t \frac{1}{n} (\mu_p n_i^2 + \mu_n n^2) dt'. \quad (3.10)$$

The differential equation, Equation (3.9), can be solved by using the integrating factor e^Q where Q is given by Equation (3.10). Formally, the solution for the electric field from Equation (3.9) is

$$E(x,t) - e^{-Q}E(x,0) = \frac{-kT}{q} e^{-Q} \int_0^t e^Q \frac{\partial Q}{\partial t} \frac{1}{n} \frac{\partial}{\partial x} dt', \quad (3.11)$$

where Q is given by Equation (3.10).

For heavily-doped substrates where the surface states are compensated by the substrate doping, $E(x,0)$ is approximately zero for all x . With this condition Equation (3.11) can be written as

$$E = \frac{-kT}{q} e^{-Q} \int_0^t e^Q \frac{\partial Q}{\partial t} \frac{1}{n} \frac{\partial n}{\partial x} dt'. \quad (3.12)$$

For substrates which are near intrinsic at the growth temperature, such as chromium-doped substrates, $E(x,0)$ would not be zero and the full form of Equation (3.11) must be used.

3.1.2 Impurity Concentrations

Combining Equations (3.2) and (3.3) for electrons gives

$$q \frac{\partial n}{\partial t} = \frac{\partial}{\partial x} \left[q\mu_n nE + qD_n \frac{\partial n}{\partial x} \right], \quad (3.13)$$

which can be written as

$$\frac{1}{D_n} \frac{\partial n}{\partial t} = \frac{\partial^2 n}{\partial x^2} + \frac{q}{kT} \frac{\partial}{\partial x} (nE). \quad (3.14)$$

Using the value for the electric field given in Equation (3.11) in Equation (3.14), the equation for determining the electron concentration can be obtained. This equation is

$$\frac{1}{D_n} \frac{\partial n}{\partial t} = \frac{\partial^2 n}{\partial x^2} - \frac{\partial}{\partial x} \left\{ ne^{-Q} \left[\int_0^t e^Q \frac{\partial Q}{\partial t} \frac{1}{n} \frac{\partial n}{\partial x} dt + \frac{q}{kT} E(x,0) \right] \right\} \quad (3.15)$$

where Q is given by Equation (3.10).

For heavily-doped substrates, Equation (3.15) becomes

$$\frac{1}{D_n} \frac{\partial n}{\partial t} = \frac{\partial^2 n}{\partial x^2} - \frac{\partial}{\partial x} \left[ne^{-Q} \int_0^t e^Q \frac{\partial Q}{\partial t} \frac{1}{n} \frac{\partial n}{\partial x} dt \right]. \quad (3.16)$$

The donor and acceptor concentrations can then be determined from

$$\frac{1}{D_j} \frac{\partial N_j}{\partial t} = \frac{\partial^2 N_j}{\partial x^2} \pm \frac{\partial}{\partial x} \left\{ N_j e^{-Q} \left[\int_0^t e^Q \frac{\partial Q}{\partial t} \frac{1}{n} \frac{\partial n}{\partial x} dt + \frac{qE(x,0)}{kT} \right] \right\} \quad (3.17)$$

where n is determined from Equation (3.16), Q is given by Equation (3.10), and the upper + sign is for the positively-charged donors, while the lower - sign is for the negatively-charged acceptors.

Although in general the time-dependent solution of Equations (3.10), (3.11), (3.15), and (3.17) must be used, at low growth rates, v , and thin epitaxial layer thicknesses, L , the ionized donors and acceptors are in equilibrium with the electric field and the time-independent solution is a good approximation. That is, the time-independent solution can be used for vL much less than D_j , the impurity diffusion coefficients.

3.2 TIME-INDEPENDENT SOLUTIONS

3.2.1 Heavily-Doped Substrate

3.2.1.1 Assumptions

For the time-independent impurity gradient model four assumptions are used which provide a reasonably good approximation to the growth of an n-layer on a heavily-doped substrate and which are sufficiently constrained to produce analytical result. The assumptions are as follows:

(1) The carrier concentration of the substrate is fixed by the substrate doping, N_s , which is greater than the carrier concentration at the growth temperature, n_i .

(2) The carrier concentration of the growing layer, n_i , is determined by the growth temperature and not by the ionized donors, N_d , and acceptors, N_a , incorporated during the growth process. That is, n_i is greater than N_d and N_a .

(3) The carrier concentration at the growth surface, n_0 , is fixed by surface states and is less than n_i .

(4) The product of growth rate, v , and epitaxial layer thickness, L , is much less than the impurity diffusion coefficients, D_j .

Practically, these assumptions approximate the growth of a very thin, lightly-doped epitaxial layer on a heavily-doped substrate with a very low growth rate.

Since the surface of the epitaxial layer is moving due to the growth process, a moving coordinate system is used. The transformation to the moving coordinate system is given by

$$\xi = x + vt = x + L, \quad (3.18)$$

where ξ is the distance from the growth surface, $-x$ is the distance from the substrate, v is the growth rate, and L is the layer thickness.

3.2.1.2 Electron Concentration

3.2.1.2.1 Solution

Since the donor and acceptor concentrations are sufficiently low, the carrier concentration of the growing layer is determined by the growth temperature, not by the ionized donors and acceptors. From Section 2.1.2.5 the epitaxial layer will be intrinsic at the growth temperature for a net donor concentration, $N_d - N_a$, less than

10^{16} cm^{-3} . This analysis should then apply for layers doped below this level.

The time-independent equation for electrons is

$$\frac{\partial n}{\partial t} = 0 = \mu_n \frac{d}{d\xi} (nE) + D_n \frac{d^2 n}{d\xi^2}, \quad (3.19)$$

from the combination of the conduction equation, Equation (3.2), and the continuity equation, Equation (3.3). Poisson's equation, Equation (3.1) for the lightly doped case is

$$\frac{dE}{d\xi} = \frac{q}{\epsilon\epsilon_0} (p - n). \quad (3.20)$$

Putting Equation (3.20) into Equation (3.19) yields,

$$\frac{nq\mu_n}{\epsilon\epsilon_0} (p - n) + \mu_n E \frac{dn}{d\xi} + D_n \frac{d^2 n}{d\xi^2} = 0 \quad (3.21)$$

For the time-independent case the electron conduction current, J_n , at most would be a constant. In this analysis for equilibrium the electron conduction current is zero. Equation (3.2) for electrons can then be written as

$$\mu_n E = - \frac{D_n}{n} \left(\frac{dn}{d\xi} \right). \quad (3.22)$$

Putting Equation (3.22) into Equation (3.21) and using

the mass action law for the generation of holes and electrons, Equation (3.5) produces

$$\frac{q\mu}{\epsilon\epsilon_0} (n_i^2 - n^2) - \frac{D_n}{n} \left(\frac{dn}{d\xi}\right)^2 + D_n \frac{d^2n}{d\xi^2} = 0 \quad (3.23)$$

This equation can be written, using Einstein's relation, in the form

$$\frac{d^2n}{d\xi^2} - \frac{1}{n} \left(\frac{dn}{d\xi}\right)^2 - \frac{A^2}{2} n^2 + \frac{B^2}{2} = 0 \quad (3.24)$$

where

$$A = \left(\frac{2q^2}{\epsilon\epsilon_0 kT}\right)^{1/2},$$

and

$$B = \left(\frac{2q^2 n_i^2}{\epsilon\epsilon_0 kT}\right)^{1/2}.$$

Equation (3.24) has solutions

$$n = \frac{B}{A} \tanh^2 \left(\frac{AB}{2} \xi + C_1 \right)$$

and

(3.25)

$$n = \frac{B}{A} \coth^2 \left(\frac{AB}{2} \xi + C_2 \right).$$

These solutions can be rewritten as

$$n = n_i \tanh^2 \left(\frac{\xi}{L_i} + C_1 \right) \quad (3.26)$$

and

$$n = n_i \coth^2 \left(\frac{\xi}{L_i} + C_2 \right) \quad (3.27)$$

where

$$L_i = \left\{ \frac{2\epsilon\epsilon_0 kT}{q^2 n_i} \right\}^{1/2} \quad (3.28)$$

3.2.1.2.2 Boundary Conditions

At the surface of the growing layer the electron concentration, n_0 , is assumed to be fixed by surface states below the intrinsic electron concentration. The solution for the electron concentration near the surface is given by Equation (3.26). At the surface ($\xi = 0$), the constant, C_1 , can be calculated, using the boundary condition $n(\xi = 0) = n_0$, as

$$\alpha = \tanh^{-1} \left(\frac{n_0}{n_i} \right)^{1/2}, \quad (3.29)$$

where C_1 equals α . The electron concentration near the surface can be written from Equation (3.26) as

$$n(\xi) = n_i \tanh^2 \left(\frac{\xi}{L_i} + \alpha \right), \quad (3.30)$$

where α is given by Equation (3.29) and L_i is given by Equation (3.28).

Near the substrate-layer interface ($\xi = L$) the electron concentration in the epitaxial layer, n_1 , is

$$n_1(\xi) = n_i \coth^2 \left(\frac{L - \xi}{L_i} + C_2 \right), \quad (3.31)$$

from Equation (3.27). This equation can be rewritten as

$$n_1(x) = n_i \coth^2 \left(\frac{-x}{L_i} + C_2 \right), \quad (3.32)$$

where $-x$ is the distance in the epitaxial layer from the interface. The electron concentration in the substrate, n_2 , can be approximated using Equation (3.26) as

$$n_2(x) = N_s \tanh^2 \left(\frac{x}{L_e} + C_3 \right) \quad (3.33)$$

where x is the distance from the interface in the substrate and

$$L_e = L_i \left(\frac{n_i}{N_s} \right)^{1/2}.$$

Since the electron concentration is continuous at the interface ($\xi = L$), the relationship between C_2 and C_3 can be found using Equations (3.32) and (3.33) as

$$\coth C_2 = \left(\frac{N_s}{n_i} \right)^{1/2} \tanh C_3. \quad (3.34)$$

The exact values of C_2 and C_3 can be calculated from

the single-valueness of the electric field at the interface ($x = 0$). This will be done in Section 3.2.1.2.1. Using the values calculated in that section, the electron concentration is plotted in Figure 3.1 for various substrate-intrinsic concentration ratios, N_s/n_i . In this figure $-x$ is the distance from the interface into the epitaxial layer and x is the distance from the interface into the substrate.

3.2.1.3 Electric Field

3.2.1.3.1 Interface

The equilibrium electric field can be calculated from Equation (3.22). Using Einstein's relation this equation can be written as

$$E(x) = - \frac{kT}{q} \left(\frac{1}{n} \right) \frac{dn}{dx} . \quad (3.35)$$

The electric field in the epitaxial layer (E_1) near the interface ($x = 0$) is obtained from Equation (3.35) as

$$E_1(x) = - \frac{4kT}{qL_i} \operatorname{csch} 2 \left(\frac{-x}{L_i} + C_2 \right) , \quad (3.36)$$

where $-x$ is the distance from the interface into the epitaxial layer and L_i is given by Equation (3.28).

The electric field in the substrate (E_2) is calculated from Poisson's equation,

$$\frac{dE_2}{dx} = \frac{q}{\epsilon\epsilon_0} (N_s - n_2) , \quad (3.37)$$

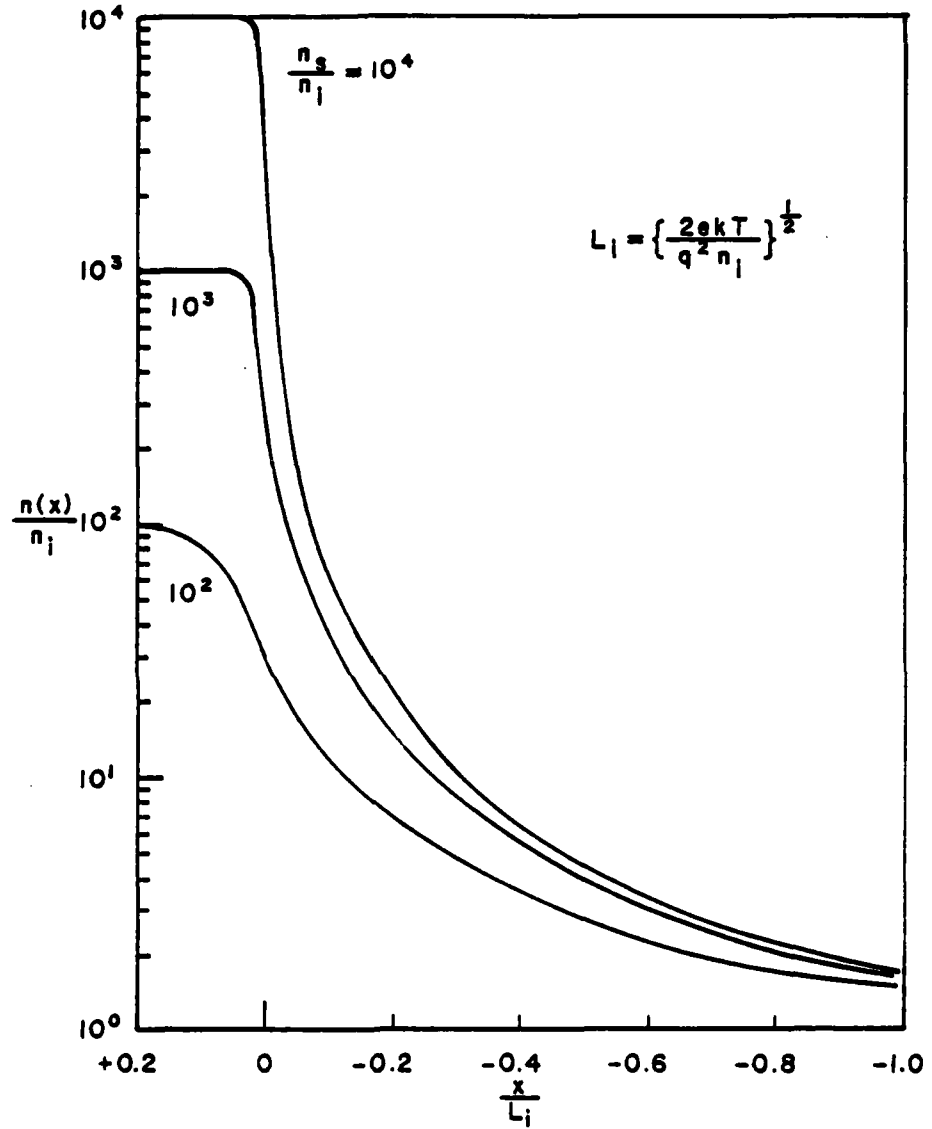


Figure 3.1 Electron concentration versus distance for various substrate-intrinsic concentration ratios, N_s/n_i . The interface is at $x=0$ and $-x$ is the distance into the epitaxial layer while $+x$ is the distance into the substrate.

where n_2 is given by Equation (3.33). Inserting Equation (3.33) into Equation (3.37) gives

$$\frac{dE_2}{dx} = \frac{qN_s}{\epsilon\epsilon_0} \operatorname{sech}^2 \left(\frac{x}{L_e} + C_3 \right), \quad (3.38)$$

where $L_e = \left(\frac{n_i}{N_s} \right)^{1/2} L_i$.

By integrating Equation (3.38) and taking the electric field far into the substrate to be zero, the electric field near the interface ($x = 0$) is obtained. This electric field is

$$E_2(x) = - \frac{2kT}{qL_e} \left\{ 1 - \tanh \left(\frac{x}{L_e} + C_3 \right) \right\}, \quad (3.39)$$

where x is the distance from the interface into the substrate.

Since the electric field must be single-valued at the interface ($x = 0$), the electric fields in the substrate, E_2 , and in the epitaxial layer, E , are equal at that point. Combining Equations (3.36) and (3.39) and setting $x = 0$ yields

$$2 \operatorname{csch} 2 C_2 = \left(\frac{N_s}{n_i} \right)^{1/2} \left\{ 1 - \tanh C_3 \right\}. \quad (3.40)$$

From Equation (3.34),

$$\tanh C_3 = \left(\frac{n_i}{N_s} \right)^{1/2} \operatorname{coth} C_2.$$

Using this equation in Equation (3.40) produces

$$2 \coth C_2 - \tanh C_2 = \left(\frac{N_s}{n_i}\right), \quad (3.41)$$

after some rearrangement. Letting $C_2 = \beta$, Equation (3.41) can be written as

$$2 \coth \beta - \tanh \beta = \left(\frac{N_s}{n_i}\right)^{1/2}. \quad (3.42)$$

From Equations (3.34), (3.36), (3.39), and (3.42) the normalized electric field is plotted in Figure 3.2 for various substrate-intrinsic carrier concentration ratios. On the normalized electric field scale 10 is approximately 4×10^5 volts/cm. The interface is located at $x = 0$, $-x$ is distance into the epitaxial layer, and $+x$ is distance into the substrate.

3.2.1.3.2 Surface

There is a similar electric field at the surface. The boundary condition for the surface is that the electron concentration is fixed at a value n_0 by the surface states. An expression for this electric field similar to Equation (3.35) is

$$E(\xi) = -\frac{kT}{q} \left(\frac{1}{n}\right) \frac{dn}{d\xi}. \quad (3.43)$$

Combining Equations (3.30) and (3.43) yields the electric

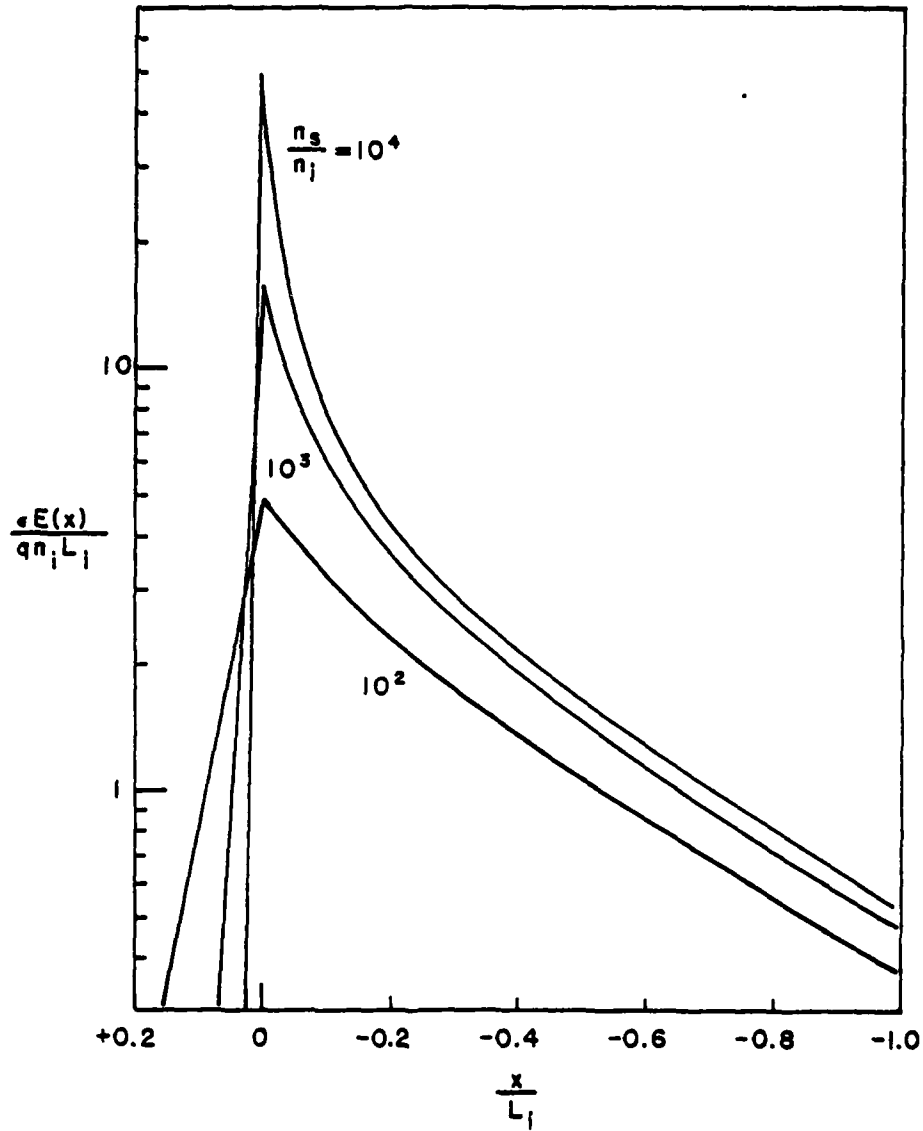


Figure 3.2 Normalized electric field versus distance for various substrate-intrinsic concentration ratios, N_s/n_i . The interface is located at $x=0$, while $-x$ is the distance into the epitaxial layer and $+x$ is the distance into the substrate.

field near the surface,

$$E(\xi) = \frac{-4kT}{qL_i} \left[\operatorname{csch} 2 \left(\frac{\xi}{L_i} + \alpha \right) \right] \quad (3.44)$$

where α is given by Equation (3.29) and L_i is given by Equation (3.28).

If we combine Equations (3.28), (3.29), (3.36), (3.42), and (3.44), the electric field in the epitaxial layer due to both the surface states and substrate doping can be obtained. This total electric field in the epitaxial layer is given by

$$E(\xi) = \frac{-4kT}{qL_i} \left[\operatorname{csch} 2 \left(\frac{\xi}{L_i} + \alpha \right) + \operatorname{csch} 2 \left(\frac{L-\xi}{L_i} + \beta \right) \right], \quad (3.45)$$

where α is determined by

$$\tanh \alpha = \left(\frac{n_0}{n_i} \right)^{1/2}, \quad (3.29)$$

β is determined from

$$2 \coth \beta - \tanh \beta = \left(\frac{N_s}{n_i} \right)^{1/2}, \quad (3.24)$$

and

$$L_i = \left(\frac{2\epsilon\epsilon_0 kT}{q^2 n_i} \right)^{1/2}. \quad (3.28)$$

With this solution for the electric field, $N_d(\xi)$ and $N_a(\xi)$ can now be determined.

3.2.1.4 Impurity Concentrations

The differential equation defining the impurity concentrations, $N_j(\xi)$, can be calculated from the conduction current equations, the continuity equations, and the electric field of Equation (3.45). Combining Equations (3.2) and (3.3) yields

$$\frac{\partial N_j}{\partial t} = D_j \frac{\partial^2 N_j}{\partial x^2} \mp \frac{q}{kT} \frac{\partial}{\partial x} (N_j E) \quad (3.46)$$

Changing Equation (3.46) to the moving coordinate system, $\xi = x + vt = x + L$, yields

$$\frac{\partial^2 N_j}{\partial \xi^2} + \left(-\frac{v}{D_j} \mp \frac{qE}{kT}\right) \frac{\partial N_j}{\partial \xi} \mp \frac{q}{kT} \frac{\partial E}{\partial \xi} N_j = \frac{1}{D_j} \frac{\partial N_j}{\partial t} \quad (3.47)$$

where the upper - sign and lower + sign are for $N_j = +N_d$ and $-N_a$, respectively. From Equation (3.47) the time-independent differential equation for $N_j(\xi)$ is

$$\frac{d^2 N_j}{d\xi^2} + \left(-\frac{v}{D_j} \mp \frac{qE}{kT}\right) \frac{dN_j}{d\xi} \mp \frac{q}{kT} \frac{dE}{d\xi} N_j = 0. \quad (3.48)$$

The solution of this equation is

$$\begin{aligned} \frac{N_j(\xi)}{N_0} &= \exp\left[\frac{v\xi}{D_j} \mp \frac{q\phi}{kT}\right] \\ &\times \left[\exp\left\{\pm \frac{q\phi_0}{kT}\right\} + \left\{ \left[-\frac{v}{D_j} \mp \frac{qE_0}{kT} + \frac{1}{N_0} \frac{dN_0}{d\xi}\right] \right. \right. \\ &\quad \left. \left. \times \int_0^\xi \exp\left[-\frac{q\xi}{D_j} \pm \frac{q\phi}{kT}\right] d\xi \right\} \right], \end{aligned} \quad (3.49)$$

where ϕ is the electrostatic potential, and ϕ_0 , E_0 , and N_0

are the potential, electric field, and donor or acceptor concentration at the growth surface. The upper and lower signs are for donors and acceptors, respectively.

As an example of the results which are obtained from this model, we use an epitaxial growth temperature of 1000 K (727°C), where $n_i = 5.8 \times 10^{16} \text{ cm}^{-3}$ and $L_i = 0.05 \text{ } \mu\text{m}$. The ratios of the substrate-intrinsic carrier concentrations, $\frac{N_s}{n_i}$, and the intrinsic-surface carrier concentrations, $\frac{n_i}{n_o}$, are 10^2 . The layer has a thickness $L = 10 L_i$ and $vL \ll D_j$. These numbers correspond to the growth of a thin n-layer on an n+ substrate at low growth rates. The results are shown in Figure 3.3. Near the growth surface ($\xi = 0$) the electric field caused by the surface states tends to attract donor impurities and repel acceptor impurities producing the impurity gradients shown. Near the layer-substrate interface ($\xi = L$) the donor impurities are repelled and the acceptor impurities are attracted by the field, producing impurity gradients in this region as well. The only effect of changing layer thickness would be to change the size of the units on the horizontal axis (provided that vL remained less than D_j).

Since donors in n-type GaAs are apparently self-compensated [18], when the sample is cooled to room temperature we expect the net donor profiles, $N_d - N_a$, to be pronounced. Assuming the high-temperature impurity

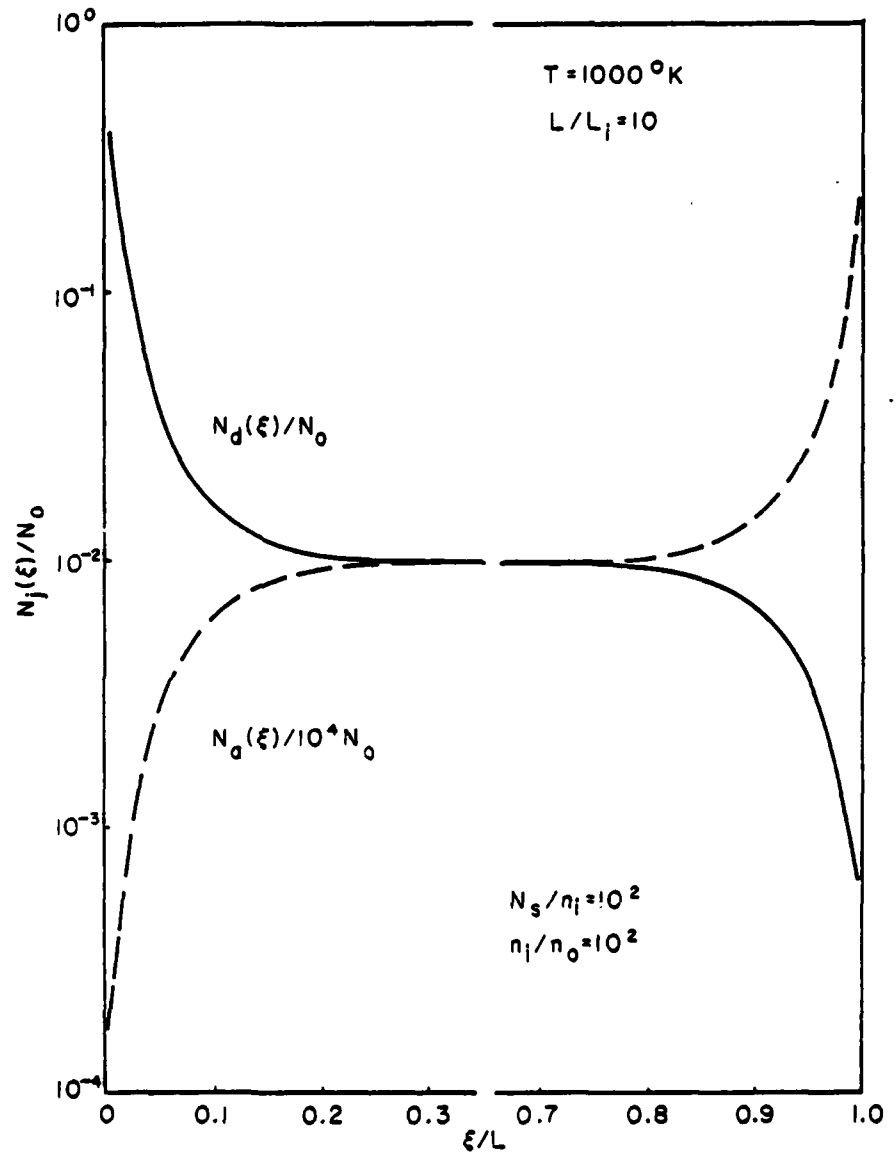


Figure 3.3 Variation of donor N_d and acceptor N_a concentrations with distance in the epitaxial layer at the growth temperature. The growth surface is at $\xi = 0$ and the substrate is at $\xi = L$.

equilibrium is frozen in, the results of Figure 3.4 are obtained at 300° K for several compensation ratios. The compensation ratios indicated are values for the middle of the layer where the gradients are zero. As can be seen, the epitaxial layer is more heavily doped near the growth surface and a thin p-type region is obtained near the layer-substrate interface.

In comparing these theoretical results with experimentally determined impurity profiles, good quantitative agreement is not expected. This is because in many GaAs epitaxial growth situations the assumption that vL is much less than D_j is not valid for donors. (Little is known about the diffusion of the compensating acceptors). Thus, a comparison with most experimental results would require the time dependent solution of the problem. In this case the donor and acceptor impurities are not in equilibrium with the electric field produced by the surface states and substrate doping, and, qualitatively, somewhat different behavior is expected.

Near the layer-substrate interface the thin p-region should be more pronounced, since, when this part of the layer is being grown, the fields from surface states and substrate doping add. However, in either case the model produces a thin p-type region which is in qualitative agreement with most experimental observations [7,12,13].

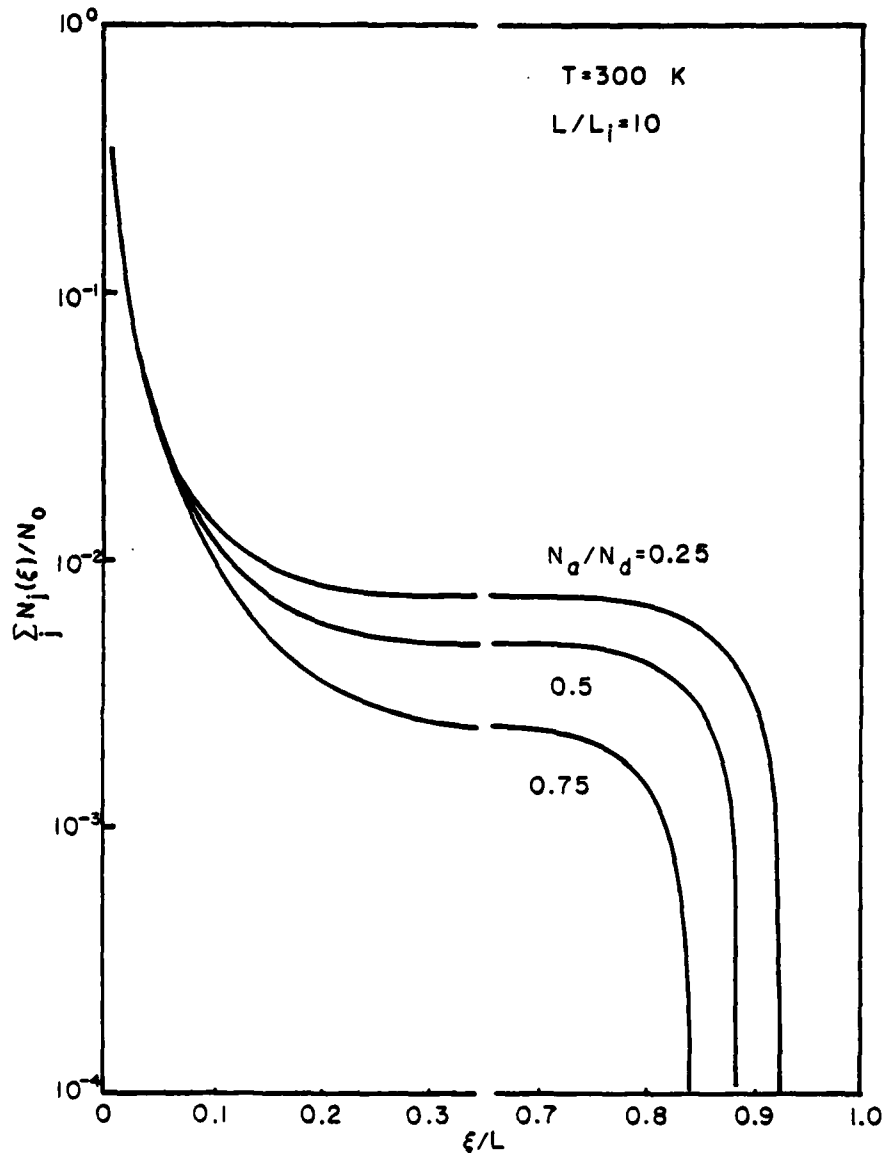


Figure 3.4 Variation of the net donor concentration ($N_d - N_a$) with distance in the epitaxial layer at room temperature for several compensation ratios. The compensation ratios indicated are values for $\xi = 0.5L$.

Also, in either case the region is expected to become more pronounced as the ratio of substrate to layer concentration increases [Equation (3.40)] in agreement with experiment [11]. In the time-dependent solution, a slight build-up of donors and a depletion of acceptors at the edge of the p-region in the epitaxial layer is expected because of the field direction. This would result in the type of profile reported by Harris *et al.* [7].

Near the growth surface the time dependent solution should produce a heavier doped n-region at the surface (similar to the time independent solution) with a build-up of acceptors and a depletion of donors at the edge of the n-region in the epitaxial layer. This type of profile near the surface has not been reported in the literature. In differential capacitance measurements, the surface region where this profile would be observed is usually depleted by the built-in field of the Schottky barrier and can be measured only under limited forward bias. Although impurity gradients near the surface have sometimes been observed in forward bias measurements, they have generally been considered as forward-bias anomalies and have received little attention. If the impurity gradient model is correct, surface impurity gradients should be common in epitaxial GaAs and could adversely affect device performance in many applications.

The impurity gradient model discussed above implies that impurity gradients at the surface and p-type regions at the layer-substrate interface are inherent to the growth process when the carrier concentrations in the substrate, growing layer, and growth surface are different at the growth temperature. That is, these problems should be encountered in most growth situations of practical interest. Considering only the p-type region at the interface, it is well known that methods have been developed to eliminate this problem. The question is, does the model predict that these methods will eliminate the problem. The most common method of eliminating the interfacial region is the use of a buffer layer between the substrate and the epitaxial layer [8]. In practice this constitutes a source of additional donors on the substrate side of the field, which according to the model, would drift into the p-region and overcompensate the acceptors. In a similar manner the model predicts that donors from out-diffusion and auto-doping [2] and *in situ* substrate etching [7] would also tend to compensate the p-region, although probably to a lesser extent than the additional donors introduced during the growth of a buffer layer. A high arsenic pressure during the initial stages of growth has also been used to eliminate the p-region. The model predicts that this could either

eliminate or enhance the p-region, depending upon the specific nature of the donors and acceptors.

In conclusion, the impurity gradient model discussed in this section explains the origin and prevalence of p-regions at n-n+ epitaxial GaAs interfaces and is consistent with many experimental observations concerning these regions. It also predicts an impurity gradient at the outer surface.

3.2.2 High Resistance Substrate

3.2.2.1 Intrinsic Layer

From the data in Section 2.2 chromium-doped substrates are near intrinsic at 1000 K. If a lightly-doped layer which is intrinsic at the growth temperature is grown on a chromium-doped substrate, as can be seen from Equation (3.42), there will be no significant electric field at the interface. Also, from Equation (3.42), if $(\frac{N_s}{n_i})$ is approximately one, then β will be infinite, which means that the second component of Equation (3.45) will be zero. Equation (3.45) will then become

$$E(\xi) = - \frac{4kT}{qL_i} \left\{ \operatorname{csch} 2 \left(\frac{\xi}{L_i} + \alpha \right) \right\}, \quad (3.50)$$

which is the electric field due to surface states only. This electric field will tend to attract donor impurities and repel acceptor impurities producing the same impurity gradient shown in Figure 3.4 near the surface. However,

there will be no significant impurity gradients at the interface. Thus, for lightly-doped epitaxial layers only a surface impurity gradient is expected.

3.2.2.2 Extrinsic Layer

Since chromium-doped substrates are slightly p-type at 1000 K, an extrinsic layer at 1000 K grown on a chromium-doped substrate should have impurity gradients at the interface. From Poisson's equation the electron concentration inside the epitaxial layer, n_e , can be expressed as

$$n_e = \frac{(N_d - N_a) + \left\{ (N_d - N_a)^2 + 4n_i^2 \right\}^{1/2}}{2},$$

where N_d is the ionized donor concentration, N_a is the ionized acceptor concentration, and n_i is the intrinsic carrier concentration. Of course, the difference between this electron concentration and the electron concentration in the slightly p-type substrate will produce an electric field at the interface. In this electric field donor impurities will be attracted towards the interface, while acceptors will be repelled. In this manner an impurity gradient will form to eliminate the electric field.

Because of surface states the electron concentration at the surface will be lower than the electron

concentration inside the epitaxial layer for all but heavily-doped epitaxial layers. From Poisson's equation the electron concentration at the surface, n_0 , can be expressed as

$$n_0 = \frac{(N_d - N_a - N_{sc}) + \left\{ (N_d - N_a - N_{sc})^2 + 4n_i^2 \right\}^{1/2}}{2}$$

where N_{sc} is the effective surface state concentration due to surface states. From Section 4 this effective surface state concentration is approximately $4 \times 10^{17} \text{cm}^{-3}$. With this surface concentration a heavily-doped layer with a net donor concentration of $4 \times 10^{18} \text{cm}^{-3}$ will have no significant electric field at the surface. However, layers with net donor concentrations of approximately 10^{17}cm^{-3} will have a difference in electron concentration between the surface and the epitaxial layer. This will produce an electric field which tends to attract donor impurities and repel acceptor impurities. Impurity gradients will, therefore, form such that the concentration gradients will counteract the electric field. This will result in a net donor concentration increase of $4 \times 10^{17} \text{cm}^{-3}$ at the surface to eliminate the electric field.

To summarize, with no outdiffusion of impurities from the substrate, growth of an extrinsic layer on a

chromium-doped substrate will result in a heavier-doped region at the interface similar to that shown in Figure 1.2. There will also be a heavier-doped region located at the surface due to surface states.

3.2.2.3 Chromium Impurity Gradient

Tuck *et al* [72] have shown that there is substantial outdiffusion of Cr into epitaxial layers grown on Cr-doped substrates. In addition, annealing experiments on Cr-doped substrates with initially uniform chromium concentrations, have indicated a redistribution of atoms producing a build-up of Cr at the surface [19,21]. This pile-up of Cr at the surface has also been observed in epitaxial layers grown on Cr-doped substrates [22,23] and in ion-implanted Cr-doped GaAs after annealing [19,20]. This Cr gradient at the surface can compensate the expected donor gradient calculated in Section 3, thus producing the zero-bias capacitance results observed on Cr-doped substrates (Section 4.2.2).

In GaAs, the neutral state of chromium is Cr^{3+} , while the acceptor state is Cr^{2+} [24,73]. Since both of the chromium species and the intentionally-added donors are positively charged they will all drift in an electric field directed towards the surface, producing impurity gradients. To obtain a simple model for chromium in GaAs, we will approximate its behavior with a single

deep acceptor near midgap [74,75]. It is well-known, however, that its effects are somewhat more complicated than this model [73,76].

To examine the formation of a chromium impurity gradient at the surface, the following assumptions are made:

(1) The carrier concentration of the growing layer, n_i , is determined by the growth temperature and not by the ionized donors, N_d , and acceptors, N_a , incorporated during the growth process or the chromium concentration, N_{Cr} , outdiffusing from the substrate. That is, n_i is greater than N_d , N_a and N_{Cr} .

(2) The carrier concentration at the growth surface, n_o , is fixed by the surface states and is less than n_i .

(3) The product of growth rate, v , and epitaxial layer thickness, L , is much less than the impurity diffusion coefficients, D_j , where j represents donors, acceptors, or chromium.

These assumptions are similar to those used before, so that the resulting electric field near the surface is

$$E(\xi) = - \frac{4kT}{qL_i} \operatorname{csch} 2\left(\frac{\xi}{L_i} + \alpha\right), \quad (3.51)$$

where α is determined by

$$\tanh \alpha = (n_o/n_i)^{1/2}. \quad (3.52)$$

The spatial variable ξ is obtained from the moving coordinate system

$$\xi = x + vt = x + L, \quad (3.53)$$

where ξ is the distance from the growth surface, and $-x$ is the distance from the substrate. From this electric field the electrostatic potential, ϕ , is

$$\phi(\xi) = \frac{2kT}{q} \ln \left| \tanh \left(\frac{\xi}{L_i} + \alpha \right) \right|. \quad (3.54)$$

To calculate the behavior of the donor, acceptor, and chromium atoms produced by this electric field, we use the current equations for ionized donors, acceptors, and both ionized and neutral chromium atoms,

$$J_j = Zq\mu_j N_j E \mp ZqD_j \frac{\partial N_j}{\partial \xi}; \quad (3.55)$$

and the continuity equations;

$$\frac{\partial N_j}{\partial t} = \mp \frac{1}{Zq} \frac{\partial J_j}{\partial \xi}. \quad (3.56)$$

The upper - signs in Equations (3.55) and (3.56) are for the positively charged donors and chromium atoms, while the lower + signs are for the negatively charged acceptors. The value of Z in these equations is one for the

singly ionized donors and acceptors, and either two or three for the chromium atoms.

Using Equation (3.55) in Equation (3.56) and Einstein's relation,

$$\mu_j = \frac{Zq}{kT} D_j, \quad (3.57)$$

yields

$$\frac{1}{D_j} \frac{\partial N}{\partial t} = \frac{\partial^2 N_j}{\partial \xi^2} - \frac{v}{D_j} \frac{\partial N_j}{\partial \xi} \mp \frac{Zq}{kT} \frac{\partial}{\partial \xi} (N_j \xi). \quad (3.58)$$

Under the assumption, $vL \ll D_j$, the system is in diffusive equilibrium and the time-independent differential equation for $N_j(\xi)$ is

$$\frac{d^2 N_j}{d\xi^2} + \left(-\frac{v}{D} \mp \frac{ZqE}{kT}\right) \frac{dN_j}{d\xi} \mp \frac{Zq}{kT} \frac{dE}{d\xi} N_j = 0. \quad (3.59)$$

The solution of Equation (3.59) is

$$\frac{N_j(\xi)}{N_0} = \exp\left(\frac{v\xi}{D_j} \mp \frac{Zq(\xi)}{kT}\right) \quad (3.60)$$

$$\times \left\{ \exp\left(\pm \frac{Zq\phi_0}{kT}\right) + \left[-\frac{v}{D_j} \mp \frac{ZqE_0}{kT} + \frac{1}{N_0} \frac{\alpha N_0}{\alpha \xi}\right]$$

$$\times \int_0^\xi \exp\left(-\frac{v\xi}{D_j} \pm \frac{Zq\phi(\xi)}{kT}\right) d\xi \right\},$$

where the electrostatic potential $\phi(\xi)$ is given by

Equation (3.54) and ϕ_0 , E_0 , N_0 are the potential, electric field, and donor, acceptor or chromium concentration at the growth surface. The upper signs are for donors and chromium atoms while the lower signs are for acceptors. The value of Z is 1 for ionized donors and acceptors, 2 for ionized chromium atoms, and 3 for neutral chromium atoms.

Quantitatively, we consider an epitaxial growth temperature of 1000 K (727°C). At this temperature $n_i = 5.8 \times 10^{16} \text{ cm}^{-3}$, and $L_i = 0.05 \text{ } \mu\text{m}$. For purposes of illustration we assume $n_i/n_0 = 10$ and $L/L_i = 10$. The results of Equation (3.60) for these conditions are shown in Figure 3.5. Near the growth surface ($\xi=0$) the electric field caused by the surface states tends to attract donor and chromium impurities and repel acceptor impurities, producing the impurity gradients shown.

Assuming that the high-temperature impurity profiles are frozen in when the growth process is terminated and the epitaxial layer is cooled to room temperature, the net donor profile, $N_d - N_a - N_{Cr}$, for 300 K is shown in Figure 3.6 for various concentrations of chromium at $\xi = 5L_i$ in the epitaxial layer. The compensation ratio $(N_a + N_{Cr})/N_d$ was fixed at 0.25 for various N_{Cr} by adjusting N_a . This net donor profile shows the formation of a high resistivity or p-type region at the

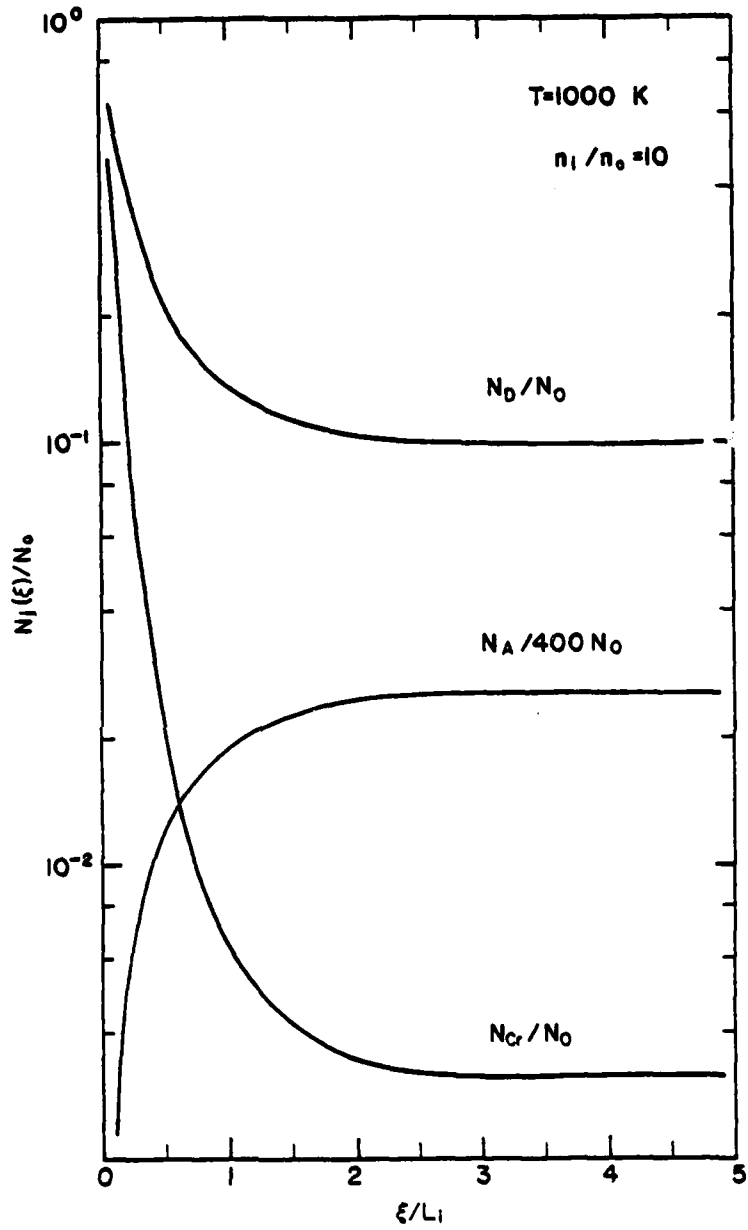


Figure 3.5 Variation of donor N_d , acceptor N_a , and chromium N_{Cr} concentrations with distance in the epitaxial layer at the growth temperature. The surface is located at $\xi = 0$.

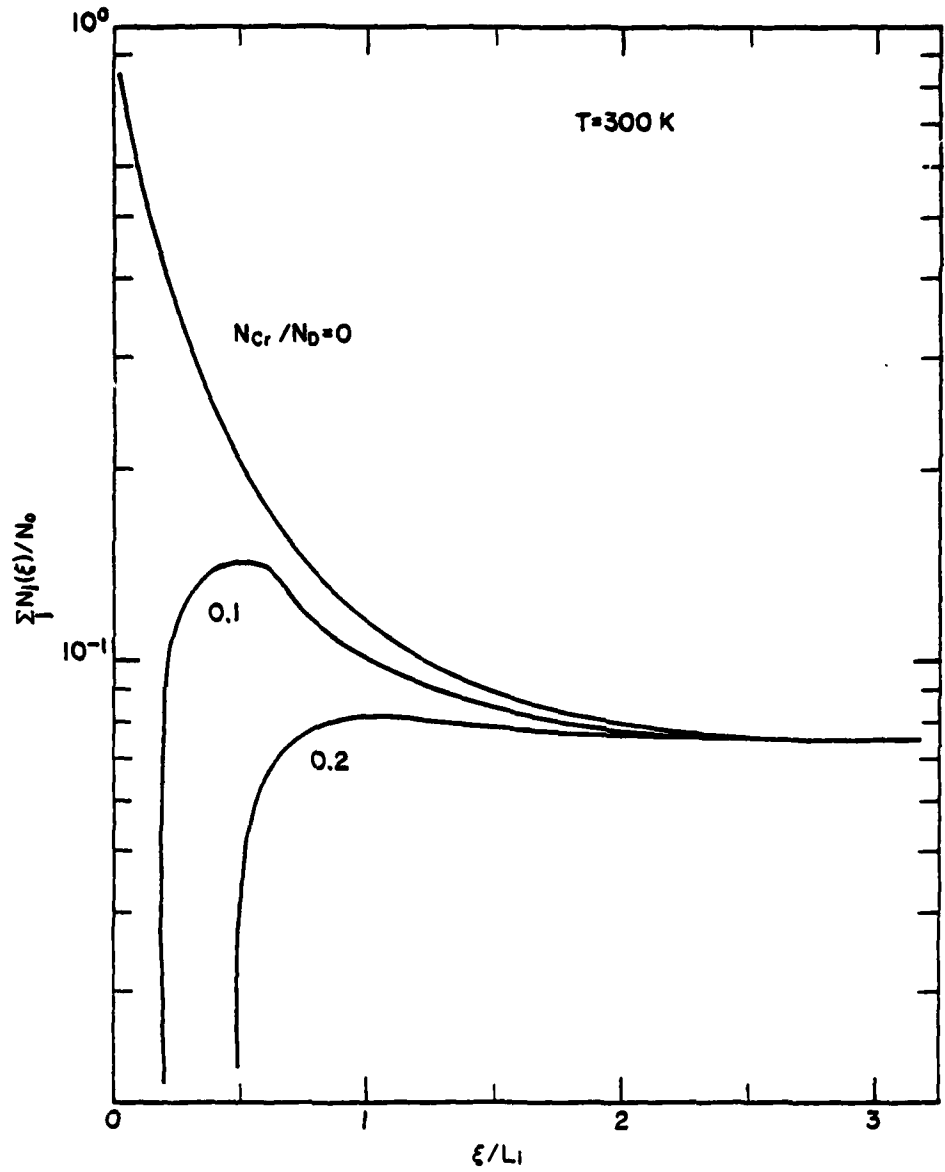


Figure 3.6 Variation of the net donor concentration ($N_d - N_a - N_{Cr}$) with distance in the epitaxial layer at room temperature for several chromium concentrations. The chromium-donor concentration ratios are values for $\xi = 5L_i$.

surface if there is chromium in the epitaxial layer. If the chromium concentration is only 3 per cent of the donor concentration at $\xi = 5L_1$, a region of negative net donor concentration will result at the surface (assuming that all of the chromium atoms are electrically active).

It has been found that not all of the chromium in GaAs is electrically active as a deep acceptor. Part of the total chromium atoms may be either neutral or at interstitial sites, acting as donors [77]. In this manner it may compensate itself [78]. Another possibility is that the high resistivity seen in Cr-doped GaAs is indirectly caused by the chromium [76]. That is, the deep acceptor may be a Cr-O complex [76].

In conclusion, the lower zero-bias capacitance observed for the as-grown portion versus the etched portion of an epitaxial layer grown on Cr-doped substrates, can be explained by a chromium impurity gradient formed due to surface states. This chromium impurity gradient can compensate the donor impurity gradient and the donor concentration of the epitaxial layer, causing the depletion width under the Schottky barrier to increase to uncover the same amount of charge. Since capacitance is inversely proportional to the depletion width, the capacitance will decrease.

This formation of a chromium impurity gradient due to surface states can also explain the observed

redistribution of chromium [19,20,21] when Cr-doped GaAs is annealed. The observed pile-up at the surface seen by Evans *et al.* [20] is typically under 1000 Å, which is the order-of-magnitude predicted by the model. It can also explain the abnormally high diffusion of chromium towards the surface during the annealing of Cr-implanted GaAs [79]. Thus, the chromium gradients observed in these annealing experiments could be caused by surface states rather than strain from the encapsulant as has been suggested [21].

4. SURFACE STATE EFFECTS

4.1 SURFACE IMPURITY GRADIENTS

4.1.1 Analysis

The model presented in Section 3.2 predicts that there will be impurity gradients at the surface of an epitaxial layer due to surface states. These impurity gradients result in the net donor profile shown in Figure 4.1 for an as-grown epitaxial layer. Unfortunately, it is difficult to obtain a direct measurement of this profile near the surface. With differential capacitance measurements this profile is already depleted at zero-bias by the built-in field of the Schottky barrier. Although in principle it is possible to probe this region with forward-bias measurements, the much larger current and resulting lower Q of the circuit produce questionable results. This prevents a direct measurement of the net donor gradient for all doping levels below $7 \times 10^{16} \text{cm}^{-3}$. However, an indirect measurement of this net donor profile can be obtained from the zero-bias capacitance of the Schottky barrier. When a Schottky barrier is formed on the surface of an as-grown epitaxial layer with a surface gradient, a certain quantity of charge under the barrier will be uncovered due to surface states. The measured zero-bias capacitance corresponds to a depletion width W_{OA} . If the surface region of the GaAs with

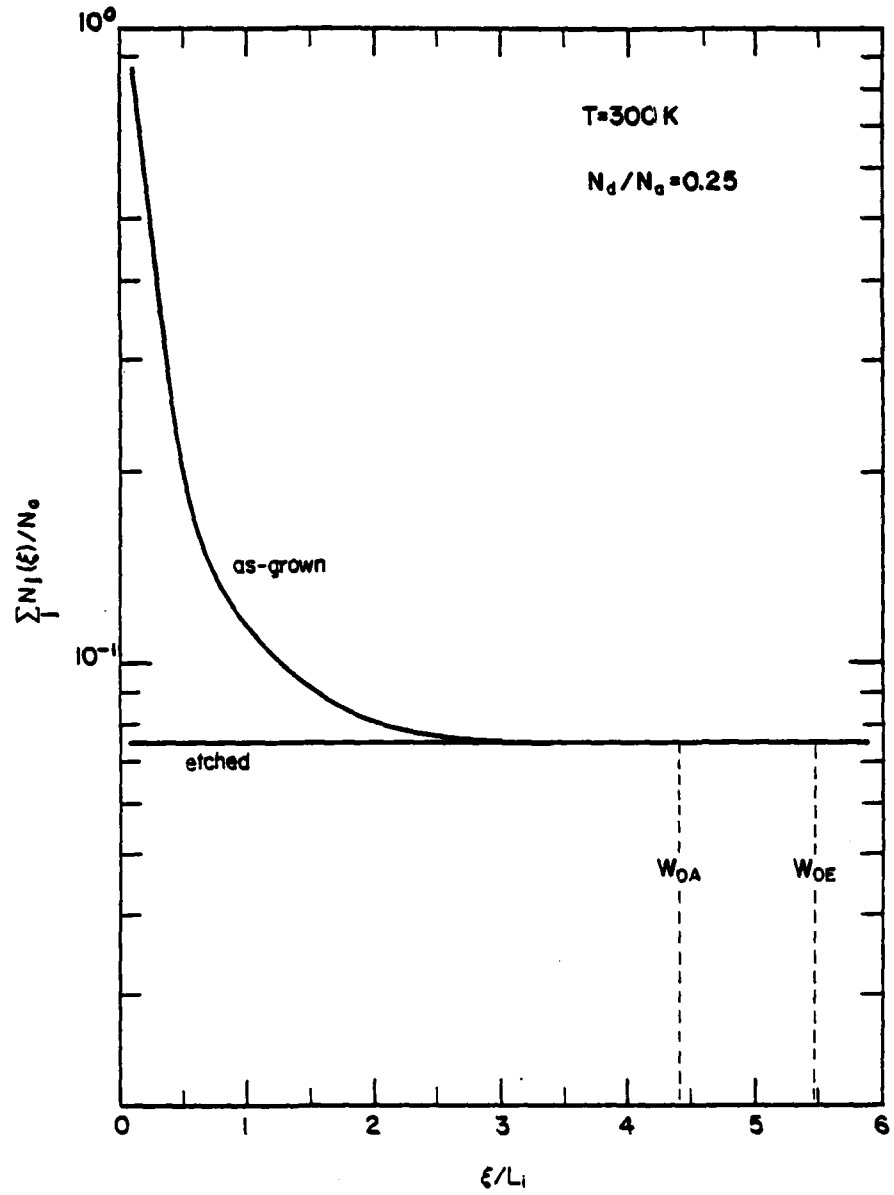


Figure 4.1 Net donor concentration ($N_d - N_a$) for as-grown and etched epitaxial layers. The values of W_{OE} and W_{OA} assumed.

this net donor gradient is then etched away, so that the net donor profile is uniform, the depletion width under the Schottky barrier must increase to W_{OE} to uncover the same total charge. The excess charge produced by the impurity gradient is the area under the as-grown profile in Figure 4.1 out to the as-grown depletion width, W_{OA} , minus the area under the etched profile also out to W_{OA} . Assuming the surface state densities are the same, this equals the area increase under the etched profile in Figure 4.1 caused by the increase of the zero-bias depletion width for the etched epitaxial layer from W_{OA} to W_{OE} . This increase in depletion width, of course, corresponds to a decrease in zero-bias capacitance for the etched layer.

For an as-grown epitaxial layer with impurity gradients at the surface, the charge uncovered beneath a Schottky barrier is

$$Q_{OA} = qA \int_0^{W_{OA}} \{N_d(\xi) - N_a(\xi)\} d\xi, \quad (4.1)$$

where $N_d(\xi)$ and $N_a(\xi)$ are taken from Section 3.2.1 as

$$N_d(\xi) = N_d(5L_i) \coth^2\left(\frac{\xi}{L_i} + \alpha\right), \text{ and} \quad (4.2)$$

$$N_a(\xi) = N_a(5L_i) \tanh^2\left(\frac{\xi}{L_i} + \alpha\right).$$

In these equations $L_i = \left(\frac{2\epsilon\epsilon_0 kT}{q^2 n_i} \right)^{1/2}$ and

$$\alpha = \tanh^{-1} \left(\frac{n_0}{n_i} \right)^{1/2}.$$

Using Equation (4.2) in Equation (4.1) yields a total uncovered charge given by

$$Q_{OA} = qA \int_0^{W_{OA}} \left[N_d(5L_i) \coth^2 \left(\frac{\xi}{L_i} + \alpha \right) - N_a(5L_i) \tanh^2 \left(\frac{\xi}{L_i} + \alpha \right) \right] d\xi \quad (4.3)$$

where W_{OA} is calculated from

$$W_{OA} = \frac{\epsilon\epsilon_0 A}{C_{OA}}. \quad (4.4)$$

C_{OA} is defined as the as-grown zero-bias capacitance.

Performing the integration in Equation (4.3) yields

$$Q_{OA} = qAL_i \left\{ (N_d - N_a) \frac{W_{OA}}{L_i} + N_d \left[\coth \alpha - \coth \left(\frac{W_{OA}}{L_i} + \alpha \right) \right] - N_a \left[\tanh \alpha - \tanh \left(\frac{W_{OA}}{L_i} + \alpha \right) \right] \right\}, \quad (4.5)$$

where $N_d \equiv N_d(5L_i)$ and $N_a \equiv N_a(5L_i)$.

For the epitaxial layer with the impurity gradients etched away, the uncovered charge is

$$Q_{OE} = qA (N_d - N_a) W_{OE}, \quad (4.6)$$

where W_{OE} is obtained from the etched zero-bias capacitance, C_{OE} , as in Equation (4.4). Since the uncovered charges, Q_{OA} and Q_{OE} , are equal, then the right-hand sides of Equations (4.5) and (4.6) are also equal. Combining Equations (4.5) and (4.6) gives

$$\begin{aligned} qAL_i (N_d - N_a) \frac{W_{OE}}{L_i} = qAL_i \left\{ (N_d - N_a) \frac{W_{OA}}{L_i} \right. \\ \left. + N_d \left[\coth \alpha - \coth \left(\frac{W_{OA}}{L_i} + \alpha \right) \right] \right. \\ \left. - N_a \left[\tanh \alpha - \tanh \left(\frac{W_{OA}}{L_i} + \alpha \right) \right] \right\}. \end{aligned} \quad (4.7)$$

Experimentally, $\frac{W_{OA}}{L_i}$ is relatively large and

$$\coth \left(\frac{W_{OA}}{L_i} + \alpha \right) \approx \tanh \left(\frac{W_{OA}}{L_i} + \alpha \right) \approx 1.$$

Equation 4.7 becomes

$$\left(\frac{W_{OE}}{L_i} - \frac{W_{OA}}{L_i} + 1 \right) = \frac{N_d \coth \alpha - N_a \tanh \alpha}{N_d - N_a}. \quad (4.8)$$

Also, $N_a \tanh \alpha$ is much smaller than $N_d \coth \alpha$.

AD-A079 594

WASHINGTON UNIV ST LOUIS MO SEMICONDUCTOR RESEARCH LAB F/G 20/12
IMPURITY AND DEFECT BEHAVIOR IN HIGH-PURITY EPITAXIAL GaAs.(U)
SEP 79 C M WOLFE, K H NICHOLS AFOSR-76-2950
59356-6 AFOSR-TR-79-1326 NL

UNCLASSIFIED

2-2
AL
26 09-84



END
DATE
FILMED
2 80
DTIC

Thus, Equation (4.8) is given approximately as

$$\coth \alpha = \left(\frac{N_d - N_a}{N_d} \right) \left\{ \frac{W_{OE}}{L_i} - \frac{W_{OA}}{L_i} + 1 \right\} . \quad (4.9)$$

Solving Equation (4.9) for α yields

$$\alpha = \coth^{-1} \left\{ \left(1 - \frac{N_a}{N_d} \right) \left[\frac{W_{OE}}{L_i} - \frac{W_{OA}}{L_i} + 1 \right] \right\} . \quad (4.10)$$

Thus, given the zero-bias capacitances and assuming a reasonable compensation ratio N_a/N_d , the surface concentration n_0 needed to produce the impurity gradients can be calculated from Equation (4.10) and the boundary condition

$$n_0 = n_i \tanh^2 \alpha . \quad (4.11)$$

With this surface electron concentration and Poisson's equation,

$$\frac{\epsilon \epsilon_0}{q} \nabla E = \sum_j N_j \quad (4.12)$$

where $N_j = + N_d, - N_a, + p, - n,$

an effective surface state concentration N_{sc} which equals

$\frac{\epsilon \epsilon_0}{q} \nabla E_0$ can be calculated. Finally, the surface state density, N_s , needed to create this surface concentration, N_{sc} , can be obtained.

4.1.2 Experiment

4.1.2.1 Heavily-Doped Substrate

Epitaxial layers were grown on n^+ GaAs substrates in an AsCl_3 -Ga- H_2 vapor-phase reactor. The substrates had a crystallographic orientation 2° off $\langle 100 \rangle$ to prevent the formation of hillocks [80]. The doping was controlled by the addition of H_2S to the reactor. In this manner, the epitaxial layers were grown to a thickness of between 4 and 7 μm with doping concentrations in the 10^{15} - 10^{16}cm^{-3} range. The samples were then removed from the reactor and a portion of each wafer was taken and etched in either $\text{H}_2\text{SO}_4:\text{H}_2\text{O}_2:\text{H}_2\text{O}$ (5:1:1) or hot Aurostrip such that 2000-3000 \AA of GaAs was removed. Sample 4 of Table 4.1 was the only sample to be etched in Aurostrip while Samples 1, 2, and 3 were etched in $\text{H}_2\text{SO}_4:\text{H}_2\text{O}_2:\text{H}_2\text{O}$. Gold Schottky barriers were formed by plating through a photoresist mask (Sample 3), evaporating (Sample 2), and sputtering (Samples 1 and 4). The values of the zero-bias capacitance measured for both the as-grown and etched portions of Samples 1 through 4 are given in Table 4.1. These capacitances are normalized to unit area. Typically, 15-25 diodes were measured on both sections of the wafers with the average values and standard deviations shown in Table 4.1. Reverse bias differential capacitance measurements on each section indicated uniform carrier

Table 4.1 Zero-bias capacitance for etched and as-grown on n^+ substrates and the surface state densities at 1000 K needed to produce these data.

Sample	Zero-bias Capacitance C_0 (nF/cm ²)		Surface State Density N_s (cm ⁻²)
	As-Grown	Etched	At 1000 K
1	16.7±0.4	13.7±0.3	5.3×10 ¹¹
2	17.3±0.5	14.6±0.4	4.8×10 ¹¹
3	19.1±0.9	15.4±0.4	5.6×10 ¹¹
4	91.3±2.0	74.0±2.5	4.5×10 ¹¹

concentrations beyond the surface regions. Using Equations (4.10) and (4.11) and assuming a compensation ratio, N_a/N_d , of 0.30, the surface concentrations were calculated for the samples listed in Table 4.1. Then, using Equation (4.12), the effective surface state concentrations were obtained. The surface state densities at 1000 K for Samples 1 through 4 are also listed in Table 4.1. From these data the average surface state density for GaAs at 1000 K was $5.1 \times 10^{11} \text{ cm}^{-2}$.

4.1.2.2 Chromium-Doped Substrate

Epitaxial layers were grown on Cr-doped GaAs substrates in an $\text{AsCl}_3\text{-Ga-H}_2$ vapor-phase reactor [39,40]. The substrates had a crystallographic orientation 2° off $\langle 100 \rangle$. With a background concentration around 10^{14} cm^{-3} , the doping of the epitaxial layers was controlled by the addition of tin to the gallium melt [81]. In this manner, the epitaxial layers were grown to a thickness of 10 and 20 μm with doping concentrations in the $10^{15}\text{-}10^{16}$ range. As before, the samples were removed from the reactor and a portion of each was etched in $\text{H}_2\text{SO}_4\text{:H}_2\text{O}_2\text{:H}_2\text{O}$ (5:1:1) such that 2000-3000 Å of GaAs was removed. Of the samples listed in Table 4.2, gold Schottky barriers were formed by plating for Samples 1 and 2 and by evaporation for Samples 3, 4, and 5. The zero-bias capacitance values normalized to unit area, are listed in Table 4.2. These data reflect impurity gradients different from

Table 4.2 Zero-bias capacitance for etched and as-grown epitaxial layers grown on Cr-doped substrates.

Sample	Zero-bias Capacitance C_0 (nf/cm ²)	
	As-grown	Etched
1	13.2±0.3	15.9±0.4
2	29.6±0.6	30.9±0.5
3	47.4±1.3	63.2±0.9
4	74.0±1.5	88.8±1.7
5	82.0±2.0	96.3±1.7

those obtained for layers grown on heavily-doped substrates. That is, the as-grown zero-bias capacitance values are lower than the etched capacitance values, indicating a higher resistivity region at the surface.

One possible explanation could be the creation of arsenic vacancies near the surface during furnace cool down. However, arsenic vacancies are believed to be donors [82,83,84] which would cause an n^+ region at the surface rather than the observed higher resistivity region.

Because of the high diffusion rate of chromium from the substrate, a more likely explanation of the data in Table 4.2 is a pile-up of chromium at the surface due to the electric field produced by surface states. Since chromium in GaAs is positively charged [24,73], the chromium should drift towards the surface, compensating the donors also drifting towards the surface.

As was demonstrated in Section 3.2.2.3, this double drift process under certain conditions can produce a high-resistivity region near the surface. The compensation of the donor impurity gradient and the donor concentration of the epitaxial layer by the chromium gradient will cause the depletion width under a Schottky barrier to increase to uncover the same amount of charge. Since capacitance is inversely proportional to the depletion width, the zero-bias capacitance will decrease, producing results similar to the data in Table 4.2.

4.2 SELF-COMPENSATION EFFECT

When the donor and acceptor concentrations are far below the intrinsic carrier concentration, the impurities are screened from each other by the intrinsic carrier concentration during incorporation into the epitaxial layer. This produces a constant compensation ratio, N_a/N_d , with increasing total impurity concentration, N_d+N_a . However, when the impurity concentrations, N_d and N_a , reach the same order-of-magnitude as the intrinsic carrier concentration, the impurities are no longer effectively screened. The interaction between the impurities then affects the incorporation of the donors and acceptors causing the compensation ratio N_a/N_d to increase. At high total impurity concentrations the acceptor concentration will equal the donor concentration.

4.2.1 Experiment

Figure 4.2 shows the donor and acceptor concentrations versus the total impurity concentration for a number of epitaxial layers doped with column IV impurities [18]. These data exhibit the expected increasing compensation ratio at high total impurity concentrations.

These epitaxial layers were grown on Cr-doped semi-insulating GaAs substrates in an $AsCl_3$ -Ga- H_2 vapor phase reactor [39,40]. The substrates had a crystallographic orientation of $\langle 211 \rangle$ Ga because this orientation incorporates the smallest number of residual impurities [42].

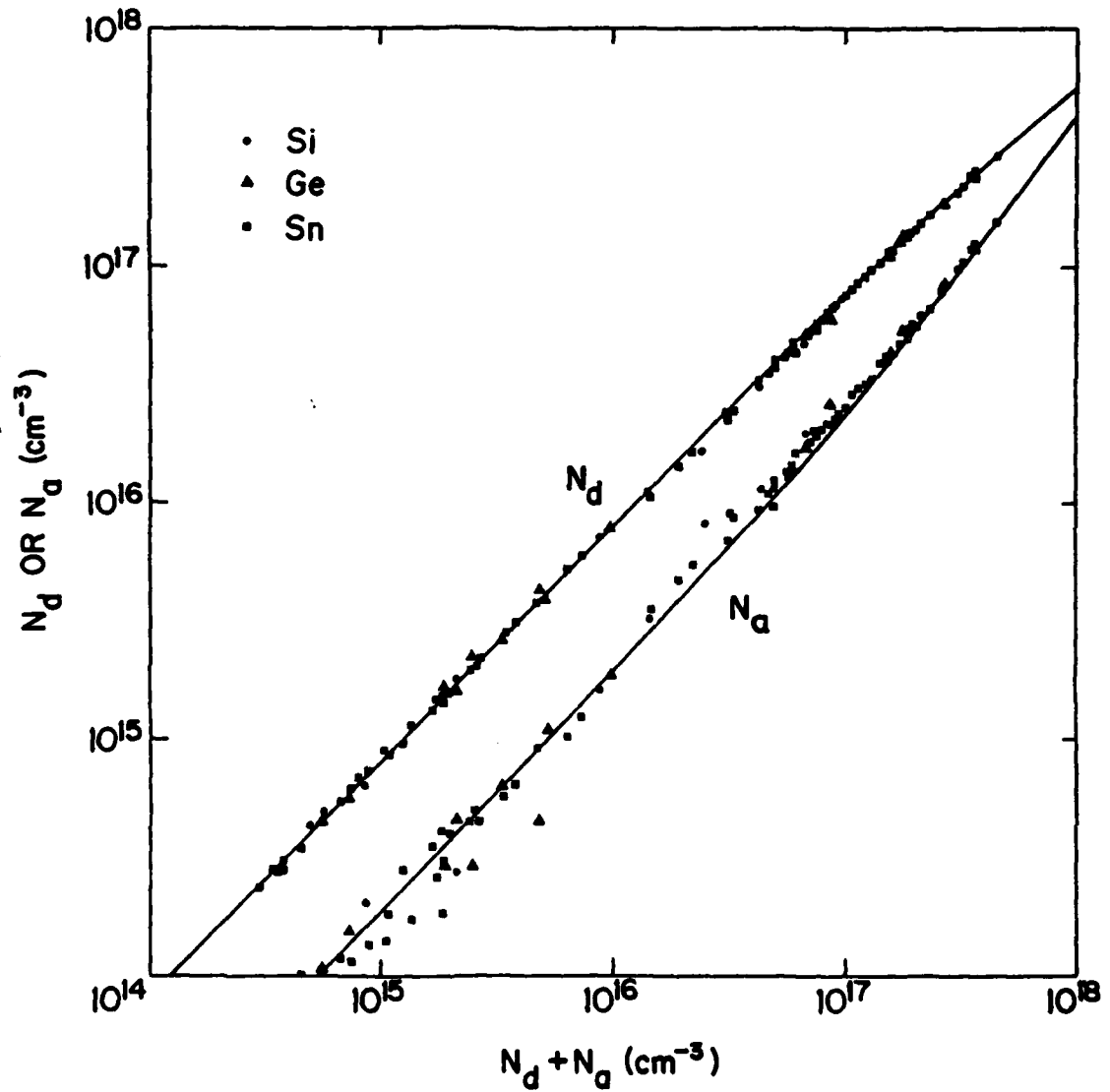


Figure 4.2 Variation of the donor concentration (N_d) and the acceptor concentration (N_a) with the total ionized impurity concentration ($N_d + N_a$) for the column-IV impurities: Si, Ge, and Sn. The lines are calculated taking into account $6.3 \times 10^{11} \text{ cm}^{-2}$ surface states.

With a background concentration around 10^{14} cm^{-3} , the doping was controlled by the addition of Si, Sn or Ge to the gallium melt [85]. In this manner epitaxial layers were grown with carrier concentrations between 5×10^{14} and $5 \times 10^{17} \text{ cm}^{-3}$. The donor concentrations, N_d , and the compensating acceptor concentrations, N_a , were determined from analyses of Hall and resistivity measurements [45].

As can be seen in Figure 4.2, both N_d and N_a increase linearly with respect to $N_d + N_a$, (N_a/N_d remains constant) at low total impurity concentrations as expected. At high concentrations, however, the compensation ratio (N_a/N_d) does not begin increasing until $N_d + N_a$ is about an order-of-magnitude larger than the intrinsic concentration. Therefore, something with a higher concentration than the intrinsic carriers is effectively screening the donor-acceptor interaction.

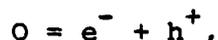
Since surface states increase the hole concentration in n-type material at the growth surface [86], surface states could effectively screen the impurities to concentrations higher than the intrinsic carrier concentration. Casey *et al.* [87] and Zechauer and Vogel [88] have used surface band bending [86] to account for several previously unexplained impurity incorporation effects in the liquid-phase epitaxial growth of GaAs. From Section 4.1.2, we see that band bending due to surface states is applicable to vapor phase epitaxy as well.

If the screening effect of surface states is taken into account, the solid lines in Figure 4.2 can be fit to the data. This will be discussed in detail in Section 4.2.2.3.

4.2.2 Analysis

4.2.2.1 Mass Action Laws

To model the incorporation of impurities into epitaxial GaAs, mass action laws for dilute solutions [89] are used. The first quasi-chemical reaction,



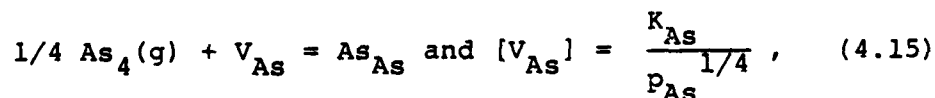
is for the generation of holes and electrons. The associated mass action law is

$$np = n_i^2, \quad (4.13)$$

where n_i is the equilibrium constant which is strongly temperature-dependent. Assuming Schottky disorder, the quasi-chemical reaction and associated mass action law for the formation of stoichiometric defects are

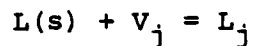
$$V_{Ga} + V_{As} = 0 \text{ and } [V_{Ga}] [V_{As}] = K_s, \quad (4.4)$$

where $[V_{Ga}]$ and $[V_{As}]$ are the concentrations of gallium and arsenic vacancies, respectively. The incorporation reaction for equilibrium with the gaseous phase can be written as



where P_{As_4} is the partial pressure of As_4 in the reactor.

The addition of an impurity, L , into the epitaxial layer is represented by

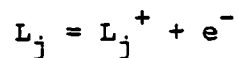


and

(4.16)

$$[L_j] = K_1 N_L [V_j],$$

where the j may be either a gallium or arsenic site and N_L is the total concentration of the impurity. Assuming a donor impurity, the ionization reaction is given by



and

(4.17)

$$nN_d = K_d [L_j].$$

Considering the self-compensation of doped n-type GaAs [18,90], there is now substantial evidence that the compensating acceptors [18,83,91-98] are impurity-defect complexes. Because of the linear increase of N_a with total added donor atoms for the data in Figure 4.2, this complex must have a donor atom associated with it. We assume that the complex is a donor atom associated with a vacancy on the same sub-lattice as the donor atom.

This acceptor complex is represented by

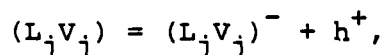


and

(4.18)

$$[(L_j V_j)] = K_2 N_L [V_j]^2.$$

The ionization of this acceptor complex is given by



and

(4.19)

$$p N_a = K_a [(L_j V_j)].$$

It should be pointed out, however, that for constant temperature and partial pressure of arsenic, the analysis in Sections 4.2.2.2 and 4.2.2.3 is independent of the type of self-compensating acceptor assumed. An amphoteric acceptor [17], or another donor-vacancy complex [94-98] will produce the same results.

Using Equations (4.14, 4.15, 4.16, and 4.17), the ionized donor concentration, N_d , is

$$N_d = \left\{ \frac{K_d K_1 K_{As}}{n p_{As}^{1/4}} \right\} N_L, \quad (4.20)$$

for incorporation of the donors on the arsenic sublattice. For incorporation of the donors on the gallium

sub-lattice the ionized donor concentration is given by

$$N_d = \left[\frac{K_d K_1 K_s P_{As}^{1/4}}{n K_s} \right] N_L \quad (4.21)$$

For constant temperature and arsenic partial pressure both Equations (4.20) and (4.21) become

$$N_d = \frac{K_d'}{n} (N_d + N_a) \quad (4.22)$$

where the total impurity concentration, $N_d + N_a = N_L$.

In a similar manner, the acceptor concentration, N_a , can be calculated using Equations (4.13, 4.14, 4.15, 4.18, and 4.19) resulting in the following:

$$N_a = \frac{n K_a K_2 K_{As}^2}{n_i^2 P_{As}^{1/2}} N_L \quad (4.23)$$

for complexes on the arsenic sub-lattice, and

$$N_a = \frac{n K_a K_2 K_s^2 P_{As}^{1/2}}{n_i^2 K_{As}^2} N_L \quad (4.24)$$

for complexes on the gallium sub-lattice. For constant arsenic partial pressure and temperature, Equations (4.23) and (4.24) can be represented by

$$N_a = n \frac{K_A'}{n_i^2} (N_d + N_a) \quad (4.25)$$

where $N_d + N_a = N_L$.

The net donor concentration can then be expressed as

$$(N_d - N_a) = \left\{ \frac{K_d'}{n} - \frac{K_a' n}{n_i^2} \right\} (N_d + N_a), \quad (4.26)$$

using Equations (4.25) and (4.22). When the impurity concentrations are small compared to n_i the layer is intrinsic and Equation (4.26) becomes $N_d - N_a = K(N_d + N_a)$, which produces constant compensation. As the carrier concentration increases at high doping levels, K_d'/n decreases while $K_a' n/n_i^2$ increases causing the compensation ratio to increase.

4.2.2.2 Charge Neutrality

If we assume no surface states, then there is no electric field at the surface and charge neutrality must be maintained. Thus, the neutrality condition is

$$n + N_a = p + N_d, \quad (4.27)$$

for the epitaxial layer. This equation can be rewritten as

$$n = \frac{(N_d - N_a) + [(N_d - N_a)^2 + 4n_i^2]^{1/2}}{2}, \quad (4.28)$$

by using Equation (4.13). From this equation, if $N_d, N_a \ll n_i$ then the electron concentration, n , is equal to the intrinsic carrier concentration.

For a total impurity concentration below 10^{16} cm^{-3} , the carrier concentration is within 5 percent of the

intrinsic concentration. From the data in Figure 4.2, the equilibrium constant K'_d in Equation (4.22) can be calculated. The calculated value of K_D is $4.90 \times 10^{16} \text{ cm}^{-3}$ with a standard deviation of $0.14 \times 10^{16} \text{ cm}^{-3}$ for 29 data points.

Similarly, from the data of Figure 4.2, the equilibrium constant K'_a of Equation (4.25) is calculated to be $1.10 \times 10^{16} \text{ cm}^{-3}$. The standard deviation of this value is $0.82 \times 10^{16} \text{ cm}^{-3}$ for 29 data points. From the data in Figure 4.2, the calculated equilibrium constants, K'_d and K'_a , and Equation (4.28), the net donor concentration can be calculated from Equation (4.26) for no surface states. This calculated net donor concentration is the dashed line shown in Figure 4.3. As can be seen, the experimental data do not agree with this calculated curve. Therefore, some charged species at a higher concentration than the intrinsic carrier must be screening the donor and acceptor impurities as they are being incorporated into the epitaxial layer.

Hurle [99] has proposed a model to explain this behavior. His model is based on a large concentration of arsenic vacancies due to Frenkel disorder on the arsenic sub-lattice. For his model the arsenic vacancy is taken to be a donor. Thus, at high temperatures the electron concentration, n , equals the ionized arsenic vacancy

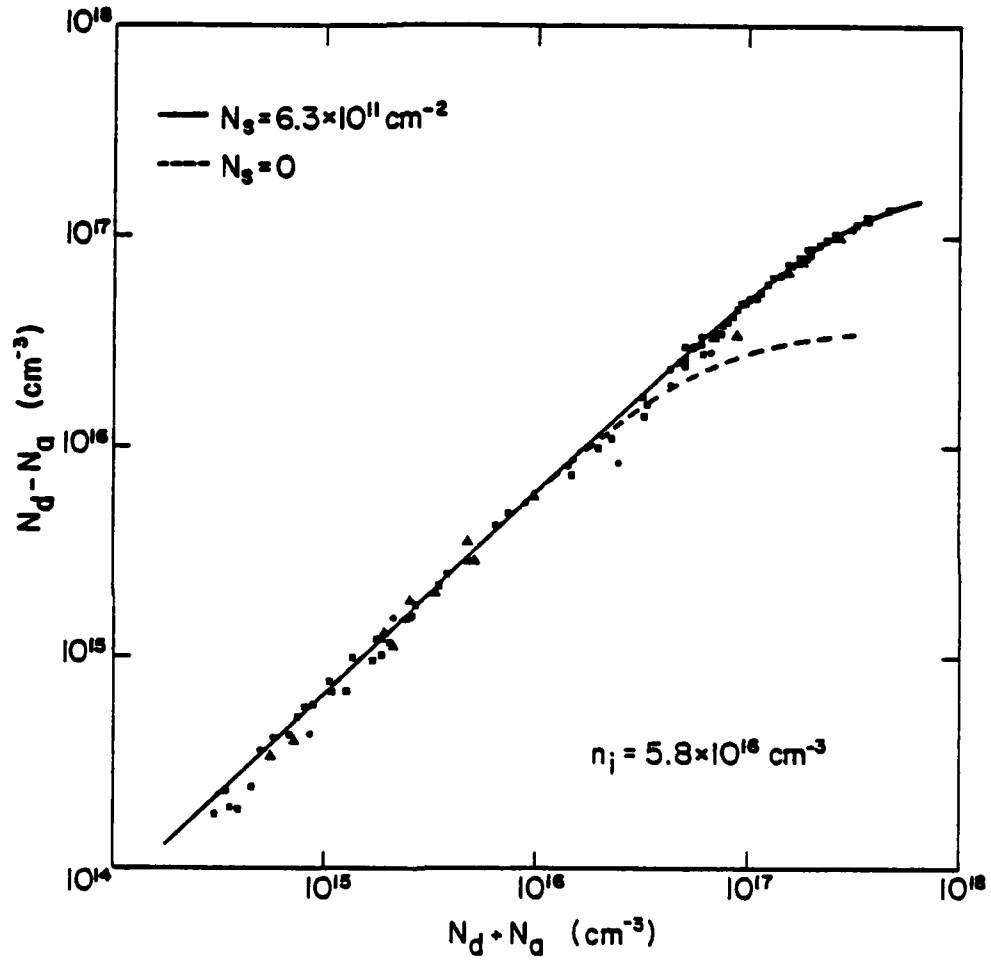


Figure 4.3 Net donor concentration ($N_d - N_a$) versus total ionized impurity concentration ($N_d + N_a$). The dashed line is calculated for zero surface states. The solid line is calculated for $6.3 \times 10^{11} \text{ cm}^{-2}$ surface states. The layers are doped with the column-IV impurities: Si (●), Ge (▲), and Sn (■).

concentration $[V_{As}^+]$ which is much greater than the intrinsic carrier concentration, n_i . This concentration of electrons and arsenic vacancies screen the donors and acceptors as they are incorporated into the epitaxial layer. At 1000 K this model requires an electron concentration of $6 \times 10^{17} \text{ cm}^{-3}$ due to the arsenic vacancies to explain the experimental data. However, the measured electron concentration at 1000 K from the high temperature Hall measurements in Section 2 is an intrinsic concentration of $5.8 \times 10^{16} \text{ cm}^{-3}$. Thus, the basic assumption of Hurle's model is incorrect.

4.2.2.3 Surface States

The effect of surface states is another explanation for the screening of impurities above the intrinsic carrier concentration. As shown in Section 3 these surface states will produce an electric field at the surface of the epitaxial layer. Because of this electric field Poisson's equation,

$$\frac{\epsilon \epsilon_0}{q} \nabla E = N_d + p - N_a - n, \quad (4.29)$$

must be used instead of charge neutrality. The gradient of the electric field at the surface corresponds to a surface concentration, N_{sc} , due to the surface states. Thus, at the surface Equation 4.29 can also be written as,

$$N_{sc} + N_a + n = N_d + p. \quad (4.30)$$

If the interaction of the impurities with the field is assumed to be at the surface only, then N_{sc} can be taken as a constant. Equation 4.30 can be solved for the electron concentration as,

$$n = \frac{(N_d - N_a - N_{sc}) + [(N_d - N_a - N_{sc})^2 + 4n_i^2]^{1/2}}{2} \quad (4.31)$$

For impurity concentrations, N_d and N_a , less than the intrinsic concentration, Equation 4.31 becomes,

$$n = \frac{[N_{sc}^2 + 4n_i^2]^{1/2} - N_{sc}}{2}, \quad (4.32)$$

which is constant for constant temperature.

To solve for the equilibrium constants K'_d and K'_a , the data in Figure 4.2 below $N_d + N_a = 10^{16} \text{ cm}^{-3}$ and an assumed N_{sc} are used. With Equations 4.22, 4.25, 4.31 and these equilibrium constants, the N_{sc} needed to fit the data above $N_d + N_a = 10^{16} \text{ cm}^{-3}$ is determined. By iteration all the data in Figure 4.2 are then fit with a self-consistent surface state concentration.

In this manner, a surface state concentration of $5.0 \times 10^{17} \text{ cm}^{-3}$ was obtained. The calculated equilibrium constants were

$$K'_d = 5.58 \times 10^{15} \pm .08 \times 10^{15} \text{ cm}^{-3}$$

and

$$K'_a = 9.62 \times 10^{16} \pm .78 \times 10^{16} \text{ cm}^{-3},$$

where the standard deviations are for 29 data points. With these constants, Equations (4.26) and (4.31) and a surface state concentration of $5.0 \times 10^{17} \text{ cm}^{-3}$ the solid line plotted in Figure 4.3 was determined. The surface state density to produce this surface concentration was $6.3 \times 10^{11} \text{ cm}^{-2}$.

4.3 CONCLUSIONS

From the previous two sections it is apparent that surface states can effect the incorporation and distribution of impurities in vapor-phase epitaxy. From Section 4.1.2.1 the average surface state density at 1000K needed to produce the surface impurity gradients observed was $5.1 \times 10^{11} \text{ cm}^{-2}$. This surface state density corresponds to a barrier height of 0.17eV for the vapor-solid interface at 1000K.

From Section 4.2.2.3 the surface state density necessary to screen the impurities was $6.3 \times 10^{11} \text{ cm}^{-2}$. A barrier height of 0.20eV is produced by this surface state density. This surprisingly good agreement between two completely different experiments tends to confirm the

effects of surface states on the growth of epitaxial layers.

The electric field produced by these surface states may also explain why GaAs epitaxial layers are self-compensated. That is the field could be expected to retard the formation of donors from donor atoms and enhance the formation of acceptors from donor-atom-vacancy complexes, thus compensating the layers.

5. SUMMARY AND CONCLUSIONS

The impurity gradient model presented in this report shows that impurity gradients are inherent to the growth process of epitaxial GaAs. That is, if all other possible mechanisms for the formation of impurity gradients were eliminated, in most epitaxial growth situations of practical interest these regions would still be observed. This impurity gradient model explains the formation of p-type regions commonly observed at the interface between an n-type epitaxial layer and an n^+ substrate. The formation of heavier-doped n-type regions located at the interface between an n-type epitaxial layer and a chromium-doped substrate can also be explained by the model.

The observed screening of impurities at concentrations above the intrinsic carrier concentration is also explained. At the surface the surface states lower the electron concentration and, therefore, increase the hole concentration. This increased hole concentration screens the impurities at the surface causing the experimentally observed compensation seen in Figure 4.3. The lower electron concentration at the surface produces band bending and an electric field near the surface.

This electric field explains the chromium pile-up observed in chromium-doped epitaxial layers and substrates.

The model predicts that this electric field will produce donor and acceptor impurity gradients near the surface. These impurity gradients are a build-up of donors and a depletion of acceptors at the surface. The electric field at the surface may also explain why GaAs epitaxial layers are self-compensated by acceptors, which are thought to be donor atom-vacancy complexes. Since there is a depleted concentration of acceptors and an excess concentration of donors at the surface, from mass action laws the formation of donor-vacancy complex acceptors will be enhanced. The electric field will cause these acceptors to drift away from the surface sustaining the depletion needed to cause enhanced complex-formation.

High temperature measurements were made on epitaxial layers and substrates to obtain quantitative results for the impurity gradient model. A self-consistent four-band model of carrier transport was used to calculate an intrinsic carrier concentration of $5.8 \times 10^{16} \text{ cm}^{-3}$ at 1000 K. From this four-band model heavily-doped substrates were calculated to still be n^+ and chromium-doped substrates were calculated to be slightly p-type at 1000 K.

Using these data p-type interfacial regions 500 to 1000 $\overset{0}{\text{A}}$ thick are predicted for the growth of lightly-doped n-type epitaxial layers on heavily-doped substrates. Interfacial regions of about this size are commonly

observed at the $n-n^+$ interfaces, as seen in Figure 1.1. This impurity gradient model should be applicable to the epitaxial growth of materials other than GaAs. It should be noted that similar $0.5 \mu\text{m}$ interfacial regions have been observed at the $n-n^+$ interface in InP [100].

By combining the experimental data for zero-bias capacitance measurements and the net donor profile predicted by the impurity gradient model, a surface state density at 1000 K was calculated. The average surface state density required to form the measured impurity gradients was $5.1 \times 10^{11} \text{cm}^{-2}$.

This calculated surface state density compares favorably with the surface state density of $6.3 \times 10^{11} \text{cm}^{-2}$ needed to explain the experimental self-compensation data of Figure 4.3. This surprisingly good agreement between two different experiments tends to confirm the impurity gradient model.

6. ACKNOWLEDGMENTS

The author would like to thank Professors C. M. Wolfe and M. W. Muller of Washington University, G. E. Stillman of the University of Illinois, and A. L. McWhorter of the Massachusetts Institute of Technology for their guidance in various aspects of this work; Drs. D. L. Rode and F. T. J. Smith for helpful discussions on high temperature carrier transport; Dr. R. E. Goldwasser and Mr. B. A. Janis of the Central Microwave Company and Miss C. M. L. Yee of Washington University for growing some of the epitaxial layers used for the experimental measurements; and Mr. S. A. Sywak for assistance with the figures.

7. BIBLIOGRAPHY

1. C. Hilsum, K. C. H. Smith, B. C. Taylor, and J. R. Knight, "C. W. X and K Band Radiation from GaAs Epitaxial Layers", *Electronics Letters* 6, 178 (1965).
2. C. M. Wolfe, A. G. Foyt, and W. T. Lindley, "Epitaxial Gallium Arsenide for High-Efficiency Gunn Oscillators", *Electrochemical Technology* 6, 208 (1968).
3. Z. J. Lemnios, "The Fabrication and Evaluation of Microwave Field Effect Transistors", Master's Thesis Washington University, May 1979.
4. F. Hasegawa and T. Saito, "Occurrence of a High Resistance Layer of Vapor Epitaxial GaAs Film-Substrate Interface", *Japanses Journal of Applied Physics* 7, 1125 (1968).
5. A. E. Blakeslee and J. E. Lewis, "Copper Contamination at the Substrate-Epitaxial Layer Interface in GaAs", *Journal of the Electrochemical Society* 116, 127C (1969).
6. J. Berrera, "The Importance of Substrate Properties on GaAs FET Performance", *Proceedings of Conference on Active Semiconductor Devices for Microwaves and Integrated Optics* (Cornell University, Ithaca, 1975) p. 135.
7. J. S. Harris, Y. Nannichi, G. L. Pearson, and G. F. Day, "Ohmic Contacts to Solution-Grown Gallium Arsenide", *Journal of Applied Physics* 40, 4575 (1969).
8. J. V. DiLorenzo, R. B. Marcus, and R. Lewis, "Analysis of Impurity Distribution in Homoepitaxial n on n^+ Films of GaAs which Contain High-Resistivity Tegions", *Journal of Applied Physics* 42, 729 (1971).
9. A. Humbert, L. Hollan, and D. Bois, Influence of the Growth Conditions on the Incorporation of Deep Levels in VPE GaAs", *Journal of Applied Physics* 47, 4137 (1976).
10. H. Sato and S. Iido, "A Thin GaAs N on N^+ Epitaxial Film with Abrupt Interface in Carrier Concentration Profile", *Japanese Journal of Applied Physics* 9, 156 (1970).

11. T. Saito and F. Hasegawa, "Cause of the High Resistance Region at Vapour Epitaxial GaAs Layer-Substrate Interface", *Japanese Journal of Applied Physics* 10, 197 (1971).
12. T. G. Blocker, R. H. Cox, and T. E. Haisty, "Interpretation of Anomalous Layers at GaAs n^+ - n^- Step Junctions", *Solid State Communications* 8, 1313 (1970).
13. J. Okamoto and S. Sakato, "Properties of a High-Resistivity Layer in Epitaxially Grown Gallium Arsenide Film", *Applied Physics Letters* 22, 446 (1973).
14. D.P. Kennedy, P. C. Murley, and W. Klenfelder, "On the Measurement of Impurity Atom Distributions in Silicon by the Differential Capacitance Technique", *IBM Journal of Research and Development*, 399 (September 1968).
15. W. Y. Lum, H. H. Wieder, W. H. Koschel, S. G. Bishop, and B. D. McCombe, "Thermal Degradation of Homoepitaxial GaAs Interfaces", *Applied Physics Letters* 30, 1 (1977).
16. H. Yamasaki, J. G. Oakes, D. L. Barrett and T. M. S. Heng, "X-band Self-Aligned Gate Power GaAs Schottky-Barrier FETs", *Proceedings of the Sixth International Symposium on Gallium Arsenide and Related Compounds, St. Louis, 1976* (Institute of Physics Conference Series 33b, London, 1977) p. 281.
17. C. M. Wolfe and G. E. Stillman, "Effect of Surface States on the Amphoteric Behavior of Sn in Vapor Epitaxial GaAs", *Solid State Communications* 12, 283 (1973).
18. C. M. Wolfe and G. E. Stillman, "Self-Compensation of Donors in High-Purity GaAs", *Applied Physics Letters* 27, 564 (1975).
19. A. M. Huber, G. Morillot, N. T. Linh, P. N. Favennec, B. Deveaud, and B. Toulouse, "Chromium Profiles in Semi-Insulating GaAs After Annealing with a Si_3N_4 Encapsulant", *Applied Physics Letters* 34, 858 (1979).
20. C. A. Evans, Jr., V. R. Deline, T. W. Sigmon, and A. Lidow, "Residtribution of Cr During Annealing of Se-Implanted GaAs", *Applied Physics Letters* 35, 291 (1979).

21. C. A. Evans, Jr., V. R. Deline, T. W. Sigmon, and A. Lidow, "Redistribution of Chromium Upon Post-Implant Annealing of Selenium Implanted GaAs", 37th Annual Device Research Conference, Boulder, Colorado, June 1979.
22. T. J. Magee, J. Peng, J. D. Hong, C. A. Evans, Jr., V. R. Deline, and R. M. Malbon, "Back Surface Gettering and Cr Out-Diffusion in VPE GaAs Layers", *Applied Physics Letters* 35, 277 (1979).
23. J. P. Duchemin, M. Bonnet, F. Koelsch, and D. Huyghe, "A New Method for Growing GaAs Epilayers by Low Pressure Organometallics", *Journal of the Electrochemical Society* 126, 1134 (1979).
24. V. Narayanamurti, M. A. Chin, and R. A. Logan, "Direct Determination of Symmetry of Cr Ions in Semi-Insulating GaAs Substrates Through Anisotropic Ballistic-phonon Propagation and Attenuation", *Applied Physics Letters* 33, 481 (1978).
25. C. M. Wolfe and K. H. Nichols, "Impurity Gradients Caused by Surface States and Substrate Doping in Epitaxial GaAs", *Applied Physics Letters* 31, 356 (1977).
26. O. G. Folberth and H. Weiss, "Herstellung und elektrische Eigenschaften Von InP und GaAs", *Zeitschrift Fuer Naturforschung* A13, 484 (1958).
27. J. M. Whelan and G. H. Wheatley, "The Preparation and Properties of Gallium Arsenide Single Crystals", *Journal of Physics and Chemistry of Solids* 6, 169 (1958).
28. L. W. Aukerman and R. K. Willardson, "High-Temperature Hall Coefficient in GaAs", *Journal of Applied Physics* 31, 939 (1960).
29. D. N. Nasledov, "Energy of Spectrum and Scattering of Current Carriers in Gallium Arsenide", *Journal of Applied Physics* 32, 2140 (1961).
30. F. E. Roberts, "High Temperature Hall Measurements on GaAs", *Physics Letters* 17, 21 (1965).
31. H. Ikoma and S. S. Wang, "Electron Trans in n-GaAs Revealed by High Temperature Hall Measurements", *Journal of the Physical Society of Japan* 27 512 (1969).

32. H. Ikoma, "High-Temperature Transport Properties of n-Type GaAs", *Journal of the Physical Society of Japan* 28, 1474 (1970).
33. V. I. Khokhlov, Yu. G. Sidorov and S. A. Dvoretiskii, "Electrophysical Properties of Non-Doped Epitaxial GaAs in the Range from 10 to 1100 K", *Physica Status Solodi* 25, 311 (1974).
34. K. Akita, H. Iida and O. Ryuzan, "Electrical Properties of n-Type Gallium Arsenide at High Temperatures", *Japanese Journal of Applied Physics* 10, 392 (1971).
35. P. Blood, "Electrical Properties of n-Type Epitaxial GaAs at High Temperatures", *Physical Review B* 6, 2257 (1972).
36. R. Zucca, "Electrical Compensation in Semi-Insulating GaAs", *Journal of Applied Physics* 48, 1987 (1977).
37. G. A. Allen, "The Activation Energies of Chromium, Iron and Nickel in Gallium Arsenide", *British Journal of Applied Physics* 1, 593 (1968).
38. F. T. J. Smith (unpublished).
39. J. R. Knight, D. Effer and P. R. Evans, "The Preparation of High Purity Gallium Arsenide by Vapour Phase Epitaxial Growth", *Solid-State Electronics* 8, 178 (1965).
40. D. Effer, "Epitaxial Growth of Doped and Pure GaAs in an Open Flow System", *Journal of the Electrochemical Society* 10, 1020 (1965).
41. D. W. Shaw, "Influence of Substrate Orientation on GaAs Epitaxial Growth Rates", *Proceedings of the Second International Symposium on Gallium Arsenide, 1968* (Institute of Physics Conference Series 7, London, 1969) p. 8.
42. C. M. Wolfe and G. E. Stillman, "High Purity GaAs", *Proceeding of the Third International Symposium on Gallium Arsenide and Related Compounds, Aachen, 1970* (Institute of Physics Conference Series 9, London, 1971) p. 1.

43. J. P. Donnelly, "Ion Implantation in GaAs", *Proceedings of the Sixth International Symposium on Gallium Arsenide and Related Compounds, St. Louis, 1976* (Institute of Physics Conference Series 33b, London, 1977) p. 166.
44. A. Lindow, J. F. Gibbons, T. Magee and J. Peng, "Multilayered Encapsulation of GaAs", *Journal of Applied Physics* 49, 5213 (1978).
45. G. E. Stillman and C. M. Wolfe, "Electrical Characterization of Epitaxial Layers" *Thin Solid Films* 31, 69 (1976).
46. W. Walukiewicz, J. Lagowski, L. Jastrzebski, M. Lichtensteiger and H. C. Gatos, "Determination of Compensation Ratios in Semiconductors from Electron Mobility and Free Carrier Absorption: GaAs", *Electro-Chemical Society Meeting, Seattle, 1978, extended abstracts* 78-1, p. 551.
47. L. J. van der Pauw, "A Method of Measuring Specific Resistivity and Hall Effect of Discs of Arbitrary Shape", *Philips Research Reports* 13, 1 (1958).
48. G. E. Stillman, C. M. Wolfe and J. O. Dimmock, "Hall Coefficient Factor for Polar Mode Scattering in n-Type GaAs", *Journal of Physics and Chemistry of Solids* 31, 1199 (1970).
49. D. L. Rode, "Electron Mobility in Direct-Gap Polar Semiconductors", *Physical Review B* 2, 1012 (1970).
50. D. L. Rode and S. Knight, "Electron Transport in GaAs", *Physical Review B* 3, 2534 (1971).
51. C. M. Wolfe, G. E. Stillman and W. T. Lindley, "Electron Mobility in High-Purity GaAs", *Journal of Applied Physics* 41, 3088 (1970).
52. D. L. Rode (private communication).
53. D. E. Aspnes, C. G. Olson and D. W. Lynch, "Ordering and Absolute Energies of the L_6^c and X_6^c Conduction Band Minima in GaAs", *Physical Review Letters* 37, 766 (1976).
54. D. E. Aspnes, "GaAs Lower Conduction-Band Minima: Ordering and Properties", *Physical Review B* 14, 5331 (1976).

55. D. E. Aspnes, "Lower Conduction Band Structure of GaAs", *Proceedings of the Sixth International Symposium of Gallium Arsenide and Related Compounds, St. Louis, 1976* (Institute of Physics Conference Series 33b, London, 1977), p. 110.
56. D. D. Sell, S. E. Stokowski, R. Dingle and J. V. DiLorenzo, "Polariton Reflectance and Photoluminescence in High-Purity GaAs", *Physical Review B* 7, 4568 (1973).
57. D. D. Sell, H. C. Casey, Jr. and K. W. Wecht, "Concentration Dependence of the Refractive Index for n- and p-Type GaAs Between 1.2 and 1.8 eV", *Journal of Applied Physics* 45, 2650 (1974).
58. M. B. Panish and H. C. Casey, Jr., "Temperature Dependence of the Energy Gap in GaAs and GaP", *Journal of Applied Physics* 40, 163 (1969).
59. C. D. Thurmond, "The Standard Thermodynamic Functions for the Formation of Electrons and Holes in Ge, Si, GaAs, and GaP", *Journal of the Electrochemical Society* 122, 1133 (1975).
60. Y. P. Varshni, "Temperature Dependence of the Energy Gap in Semiconductors", *Physica* 34, 149 (1967).
61. A. Onton, R. J. Chicotke and Y. Yacoby, *Proceedings of the 11th International Conference on the Physics of Semiconductors, Warsaw* (PWN-Polish Scientific, Warszawa, 1972). p. 1023.
62. D. Auvergne, J. Cammassel, H. Mathieu and M. Cardona, "Temperature Dependence of the Band Structure of Germanium- and Zinc-Blende-Type Semiconductors", *Physical Review B* 9 5168 (1974).
63. P. J. Dean, G. Kaminsky and R. B. Zetterstorm, "Intrinsic Optical Absorption of Gallium Phosphide Between 2.33 and 3.12 eV", *Journal of Applied Physics* 38, 3551 (1967).
64. D. E. Aspnes and A. A. Studna, "Schottky-Barrier Electroreflectance: Application to GaAs", *Physical Review B* 7, 4605 (1973).
65. G. E. Stillman, C. M. Wolfe and J. O. Dimmock, "Magnetospectroscopy of Shallow Donors in GaAs", *Solid State Communications* 7, 921 (1969).

66. H. Ehrenreich, "Band Structure and Transport Properties of Some 3-5 Compounds", *Journal of Applied Physics* 32, 2155 (1961).
67. G. D. Pitt and J. Lees, "Electrical Properties of the GaAs X_{1c} Minima at Low Electric Fields from a High-Pressure Experiment", *Physical Review B* 2, 4144 (1970).
68. C. Hilsum and J. Welborn, "Mixed Scattering in III-V Compounds", *Journal of the Physical Society of Japan Supplement* 21, 532 (1966).
69. W. Fawcett, A. D. Boardman and S. Swain, "Monte Carlo Determination of Electron Transport Properties in Gallium Arsenide", *Journal of Physics and Chemistry of Solids* 31, 1963 (1970).
70. C. Herring, "Transport Properties of a Many-Valley Semiconductor", *Bell System Technical Journal* 34, 237 (1955).
71. M. G. Crawford, W. O. Groves, A. H. Herzog and D. E. Hill, "Electroluminescence and Electrical Properties of High-Purity Vapor-Grown GaP", *Journal of Applied Physics* 42, 2715 (1971).
72. B. Tuck, G. A. Adegboyega, P. R. Jay and M. J. Cardwell, "Out-Diffusion of Chromium from GaAs Substrates", *Proceedings of the Seventh International Symposium on Gallium Arsenide and Related Compounds, St. Louis, 1978* (Institute of Physics Conference Series 45, London, 1979). p. 114.
73. Alice L. Lin and Richard H. Bube, "Photoelectronic Properties of High-Resistivity GaAs:Cr", *Journal of Applied Physics* 47, 1859 (1976).
74. S. S. Li and C. I. Huang, "Investigation of the Recombination and Trapping Process of Photoinjected Carriers in Semi-Insulating Cr-Doped GaAs Using PME and PC Methods", *Journal of Applied Physics* 43 1757 (1972).
75. G. R. Cronin and R. W. Haisty, "The Preparation of Semi-Insulating Gallium Arsenide by Chromium Doping", *Journal of the Electrochemical Society* 111, 874 (1964).

76. J. B. Mullin, D. J. Ashent, G. G. Roberts and A. Ashby, "Analysis of Deep Impurity Levels in Semi-Insulating Gallium Arsenide", *Proceedings of the Sixth International Symposium on Gallium Arsenide and Related Compounds, Edinburgh, 1976* (Institute of Physics Conference Series 33a, London, 1977) p. 91.
77. R. F. Broom, "Photoconductivity of Chromium-Doped Gallium Arsenide", *Journal of Applied Physics* 38, 3483 (1967).
78. J. W. Allen, "Gallium Arsenide as a Semi-Insulator" *Nature* 187, 403 (1960).
79. B. Deveaud and P. N. Favennec, "Photoluminescence from Chromium in GaAs", *Solid State Communications* 24, 473 (1977).
80. A. E. Blakeslee, "Effects of Substrate Misorientation in Epitaxial GaAs", *Transactions of the Metallurgical Society of AIME* 245, 577 (1969).
81. C. M. Wolfe, G. E. Stillman, and W. T. Lindley, "Tin Doping of Epitaxial Gallium Arsenide", *Proceedings of the International Symposium on GaAs, Dallas, 1968* (Institute of Physics and the Physical Society, London, 1969) p. 43.
82. S. Y. Chiang and G. L. Pearson, "Properties of Vacancy Defects in GaAs Single Crystals", *Journal of Applied Physics* 46, 2986 (1975).
83. D. T. J. Hurle, "Impurity-Point Defect Complexes in GaAs", *Proceedings of the Sixth International Symposium on Gallium Arsenide and Related Compounds, Edinburgh, 1976* (Institute of Physics Conference Series 33a, London, 1977) p. 113.
84. R. M. Logan and D. T. J. Hurle, "Calculations of Point Defect Concentrations and Nonstoichiometry in GaAs", *Journal of Physics and Chemistry of Solids* 32, 1739 (1970).
85. C. M. Wolfe, G. E. Stillman and D. M. Korn, "Residual Donors in High-Purity GaAs", *Proceedings of the Sixth International Symposium of Gallium Arsenide and Related Compounds, St. Louis, 1977* (Institute of Physics Conference Series 33b, London, 1977) p. 120.

86. R. L. Longini and R. F. Greene, "Ionization Interaction Between Impurities in Semiconductors and Insulators", *Physical Review* 102, 992 (1956).
87. H. C. Casey, Jr., M. B. Panish and K. B. Wolfstien, "Influence of Surface Band Bending on the Incorporation of Impurities in Semiconductors: Te in GaAs", *Journal of Physics and Chemistry of Solids* 32, 571 (1970).
88. K-H Zschauer and A. Vogel, "Dependence of Impurity Incorporation on Growth Rate and Crystal Orientation During GaAs Liquid-Phase Epitaxy", *Proceedings of the Third International Symposium of Gallium Arsenide and Related Compounds, Aachen, 1970* (Institute of Physics Conference Series 9, London, 1971) p. 11.
89. F. A. Kroger, *The Chemistry of Imperfect Crystals Vol. 2* (North-Holland, Amsterdam, 1973) p. 73.
90. E. S. Yurova, E. V. Solov'eva, E. M. Kistova, L. I. D'yakonov, M. I. Iglitsyn, and M. N. Kevorkov, "Self-Compensation of Donors in Gallium Arsenide and in GaAs_{1-x}P_x Solid Solutions", *Soviet Physics-Semiconductors* 6, 426 (1972).
91. E. V. Solov'eva, V. V. Karataev, M. G. Mil'vidskii, and G. A. Nemtsova, "Compensation in Gallium Arsenide Single Crystals Containing Group IV Elements", *Soviet Physics-Semiconductors* 7, 1417 (1974).
92. D. T. J. Hurle, "Solubility and Point Defect-Dopant Interactions in GaAs-11", *Journal of Physics and Chemistry of Solids* 40, 639 (1978).
93. E. W. Williams, "Evidence for Self-Activated Luminescence in GaAs: The Gallium Vacancy-Donor Center", *Physical Review* 168, 922 (1968).
94. C. J. Hwang, "Optical Properties of n-Type GaAs. 11. Formation of Efficient Hole Trans During Annealing in Te-Deped GaAs" *Journal of Applied Physics* 40, 4584 (1969).
95. R. M. Logan, "Analysis of Heat Treatment and Formation of Gallium-Vacancy-Tellurium Complexes in GaAs", *Journal of Physics and Chemistry of Solids* 32, 1755 (1970).

96. B. K. Shin, "Electrical Properties of Te-Implanted GaAs", *Journal of Applied Physics* 47, 3612 (1976).
97. D. T. J. Hurle, "Solubility and Point Defect-Dopant Interactions in GaAs-1", *Journal of Physics and Chemistry of Solids* 40, 627 (1978).
98. M. B. Panish, "The System Ga-As-Sn: Incorporation of Sn into GaAs", *Journal of Applied Physics* 44, 2659 (1973).
99. D. T. J. Hurle, "Revised Calculation of Point Defect Equilibria and Non-Stoichiometry in Gallium Arsenide", *Journal of Physics and Chemistry of Solids* 40, 613 (1978).
100. B. Jehl, F. Raisch, K. W. Benz, and M. H. Pilkuhn, "Schottky Contacts on InP: Determination of Carrier Profiles in VPE and LPE Layers", 153rd Electrochemical Society Meeting, Seattle, Washington, May 1978.